TMEM70 promotes ATP synthase assembly within cristae via transient interactions with subunit c

Hela Bahri[#,1,2,3], Jérémie Buratto[#,1,2,4], Manuel Rojo[1,2], Jim Dompierre[1,2], Bénédicte Salin[1,2], Corinne Blancard[1,2], Sylvain Cuvellier[1,2], Marie Rose[1,2], Amel Ben Ammar Elgaaied[1,2,3], Emmanuel Tetaud[1,2,5], Jean-Paul di Rago[1,2], Anne Devin[1,2], Stéphane Duvezin-Caubet[1,2,]*

Author information:
[1]Université Bordeaux, IBGC, UMR 5095, F-33000 Bordeaux, France
[2]CNRS, IBGC, UMR 5095, F-33000 Bordeaux, France
[3]Laboratoire de génétique, Immunologie et Pathologie Humaine, Faculté des sciences de Tunis – Université Tunis–El Manar FST, Tunis, Tunisie
[4]Université Bordeaux, CNRS, IPB, CBMN (UMR 5248), Institut Européen de Chimie et Biologie, 2 rue Robert Escarpit, F-33600 Pessac , France.
[5]Laboratoire de Microbiologie Fondamentale et Pathogénicité UMR-CNRS 5234, 146 rue Léo Saignat, CEDEX F-33076 Bordeaux, France.
[#]These authors contributed equally to this work and are listed in alphabetical order
*For correspondence: stephane.duvezin-caubet@ibgc.cnrs.fr

Running title: role of TMEM70 in ATP synthase assembly

Abstract

Mitochondrial ATP-synthesis is catalyzed by F1Fo-ATP synthase, an enzyme of dual genetic origin. TMEM70, a transmembrane protein mutated in neonatal encephalo-cardiomyopathies, is required for assembly/stability of ATP-synthase, but its precise role remains largely unknown. Herein, we demonstrate a role of TMEM70 in the formation of the c-ring (an oligomer of 8 c-subunits/Su.c) essential for Fo-mediated proton transport. Immunoprecipitation and two-dimensional blue-native/SDS-PAGE reveal interactions between TMEM70 and Su.c not yet assembled into the ATP synthase, and provide evidence for oligomerization of TMEM70 into homo-oligomers of 8 TMEM70 dimers. Analysis of ATP-synthase assembly in cells devoid of TMEM70, mitochondrial DNA or F1 subunits indicate that TMEM70 oligomers provide a scaffold for c-ring assembly, regardless of the presence of other ATP synthase subunits or of mitochondrial bioenergetics status. Expansion super-resolution microscopy depicting mitochondrial ultrastructure reveals the specific localization of TMEM70 within inner membrane cristae. This indicates that ATP synthase, localizing to the edge of cristae, is assembled within inner cristae membranes rather than at the inner boundary membrane that is apposed to the outer membrane.

Keywords: ATP synthase / ATP5G / Biogenesis / Cristae / Human mitochondria

Introduction

In non-chlorophyllian eukaryotes, most of the ATP is produced through oxidative phosphorylation in mitochondria. In this process, the ATP synthase uses the electrochemical proton gradient generated by the respiratory chain as the driving force to synthesize ATP from ADP and Pi (Mitchell, 1961). The mitochondrial ATP synthase is a rotary motor embedded in the inner membrane (Walker, 2013). It is made of 16 different polypeptides in mammals of which two are synthesized inside mitochondria from mitochondrial DNA/mtDNA-encoded genes (ATP6/Su.a and ATP8/Su.A6L) (Fearnley & Walker, 1986). All others are synthesized in the cytosol from nuclear genes and imported post-translationally (see Jonckheere *et al*, 2012; Kucharczyk *et al*, 2009 for reviews). The subunits are organized in two distinct domains, an extrinsic matrix domain (F1) and a membrane-embedded domain (Fo) connected by a central axis and a peripheral stalk (Walker, 2013) (Fig.2E). Passage of protons through the membrane domain involves both subunit a (Su.a) and subunit c (Su.c). This generates the rotation of a cylinder made of 8 subunits c (the c-ring) together with the central stalk subunits of F1 (γ, δ, and ε); this ensemble forms the rotor of the enzyme. Rotation of the central stalk within the catalytic head of F1, a hetero-hexamer of three Su.Alpha and three Su.Beta, induces conformational changes that allow the binding of ADP and Pi, the formation of ATP, and its release. The peripheral stalk (made of Su.OSCP, b, d, F6) holds the catalytic head on the one side and is anchored in the membrane on the other side where it binds to Su.a, A6L, and the other subunits of the complex including supernumerary subunits (Su.f, g, e, DAPIT, 6.8PL) with no equivalent in bacterial ATP synthase. The monomeric complexes associate in dimers via their membrane portion and those dimers assemble in rows along the edge of cristae (Strauss *et al*, 2008; Davies *et al*, 2011; Dudkina *et al*, 2010).

The biogenesis of the mitochondrial enzyme is a challenging process that has been thoroughly investigated in yeast and mammals (Jonckheere *et al*, 2012; Kucharczyk *et al*, 2009; Rak *et al*, 2009; He *et al*, 2018): polypeptides of dual genetic origin must be synthesized in the cytosol and in the mitochondrial matrix and must be assembled in an ordered pathway to avoid accumulation of partial intermediates that could dissipate the proton gradient or hydrolyze ATP in a futile way (Duvezin-Caubet *et al*, 2003, 2006b). The assembly of the ATP synthase is assumed to start with the separate formation of the F1 and the c-ring. Those two modules would join to form a F1-c intermediary complex. The peripheral stalk would assemble separately and next associate with the F1-c complex together with supernumerary subunits g and e (He *et al*, 2018; Habersetzer *et al*, 2013). The mtDNA-encoded subunits a and A6L would then be added together with the supernumerary subunits 6.8PL and DAPIT.

In many cases defects in OXPHOS complex biogenesis lead to proteolytic clearance of unassembled subunits by mitochondrial protein quality-control systems (Voos, 2013; Vazquez-Calvo *et al*, 2020). For instance, defective assembly of the F1 catalytic head leads to a strong reduction in levels of all subunits of the complex (De Meirleir *et al*, 2004; Rak *et al*, 2011) except for Su.c indicating that free c-ring is a stable independent entity (Havlícková *et al*, 2010; Jonckheere *et al*, 2013; Pecina *et al*, 2018). In the absence of Su.c the assembly of F1 can still proceed, and F1 can be found associated with peripheral stalk subunits (He *et al*, 2017b). Defective assembly at later steps, for instance due to the absence of some nuclear-encoded peripheral stalk subunits, lead to the accumulation of F1-c subcomplexes (He *et al*, 2018; Habersetzer *et al*, 2013; Fujikawa *et al*, 2015; He *et al*, 2017a), and similar assemblies

also comprising peripheral stalk subunits were detected in cells devoid of mtDNA-encoded subunits (Carrozzo *et al*, 2006; He *et al*, 2017b; Nijtmans *et al*, 1995; Wittig *et al*, 2010).

Some assembly steps require specific factors that are not part of the final complex. For instance, ATPAF1 and ATPAF2 are evolutionary conserved proteins required for assembling the Su.Beta and Su.Alpha hexamer (Wang *et al*, 2001). In mammals another protein called TMEM70, not present in yeast, was linked to ATP synthase biogenesis after mutations in its gene were associated with neonatal encephalo-cardiomyopathies induced by low levels of functional ATP synthase (Cízková *et al*, 2008). Since this first report in 2008, a number of other patients with pathogenic mutations in TMEM70 have been reported worldwide making these mutations the most frequent cause of ATP synthase deficiencies of nuclear origin (Magner *et al*, 2015; Torraco *et al*, 2012). In this study we unveil the oligomeric structure of TMEM70 and we demonstrate that TMEM70 protects Su.c from degradation and supports the assembly of the c-ring within cristae domains of the inner mitochondrial membrane.

Results

TMEM70 is an inner membrane protein

Analysis of TMEM70 primary structure using several algorithms (Käll *et al*, 2007; Krogh *et al*, 2001; Fukasawa *et al*, 2015) predicts a cleavable N-terminal mitochondrial targeting sequence, two transmembrane segments and a C-terminal hydrophilic domain (Fig.1A). The predicted sizes of the precursor and mature protein are 29kDa and 20.7kDa, respectively. We generated antibodies against a mixture of two distinct peptides respectively located upstream of the transmembrane segments and at the C-terminus (Fig.1A); reactivity of the sera towards the two peptides was validated by ELISA (Supp. Fig.1A). We cloned TMEM70 cDNA into a lentiviral vector independently co-expressing the DsRed fluorescent marker targeted to mitochondria (mitoDsRed) (Frank *et al*, 2012). Transduced 143B cells were FACS-sorted according to their red fluorescence in order to obtain a homogeneous population stably expressing TMEM70 and mitoDsRed. Our antibodies allowed us to detect a protein of the expected size in total cellular extracts, which levels are increased in transduced cells expressing exogenous TMEM70 (Supp Fig.1B). To define the location and topology of TMEM70, we performed cell fractionation experiments, using specific protein markers of different subcellular compartments (Fig.1B). Endogenous TMEM70 was detected almost exclusively in the crude mitochondrial fraction and a very similar profile was obtained for the ATP synthase subunit Beta confirming the mitochondrial subcellular localization of TMEM70 established previously (Hejzlarová *et al*, 2011; Jonckheere *et al*, 2011; Kratochvílová *et al*, 2014). We obtained similar results with transduced cells in which TMEM70 is overexpressed, which ruled out mistargeting and mislocalization of exogenous TMEM70 (Supp Fig.2). Moreover, endogenous TMEM70 behaved like an integral membrane protein after salt or carbonate treatment similarly to the outer membrane protein VDAC (Fig.1C). The cytochrome *c*, a protein that is peripherally associated with the inner membrane, was as expected released in the soluble fraction by these treatments. TMEM70, like cytochrome *c*, became accessible to proteinase k after rupturing the outer membrane by osmotic swelling while the matrix-localized ATP synthase subunit Beta remained intact, showing that the integrity of the inner membrane was preserved (Fig.1D). These results indicate that TMEM70 is an integral protein of the inner membrane with domains exposed to the intermembrane

space. Altogether, these data led us to propose a topological model for TMEM70 (Fig.1E) in agreement with previous studies (Jonckheere *et al*, 2011; Kratochvílová *et al*, 2014).

The knockdown of TMEM70 leads to reduced amounts of functional ATP synthase
In order to characterize the consequences of the loss of TMEM70, we first used a knock-down strategy in which TMEM70 was silenced using doxycycline-inducible shRNAs. A HEK293T-based stable cell line transduced with our lentiviral constructs was obtained and used to study the kinetics of TMEM70 disappearance within the first days of doxycycline treatment (Fig.2A). The levels of TMEM70 decreased rapidly to 20% after 3 days and less than 10% after 6-9 days. By contrast, the levels of Su.Beta remained stable during the first 3 days, decreased to 50-60% between days 3 and 5 and remained stable for the following days (Fig.2A). It is to be noticed that cells did not stop dividing at any time during the experiment. In experiments with later timepoints - where TMEM70 was virtually undetectable - the levels of Su.Beta but also of other F1 and Fo subunits (see Fig.2E for a schematic view of the ATP synthase) were stably reduced around 40-50% while the abundance of the outer membrane VDAC remained unaltered (Fig.2BC). Consistently, probing ATPase activity in Blue Native gels revealed lower levels of assembled and functional ATP synthase in the TMEM70 knock-down cells (Fig.2D). These results suggest that TMEM70 levels must decrease below some threshold level before the abundance of the ATP synthase becomes significantly diminished. It can be inferred that while TMEM70 is not essential for assembly/stability of the ATP synthase, it enables much higher enzyme yields required to sustain life-compatible ATP synthesis rates.

The absence of TMEM70 specifically impacts the ATP synthase with a marked decrease in subunit c levels
In order to further characterize the consequences of the loss of TMEM70, we generated by CRISPR/Cas9 TMEM70 knock-out cells from the HEK293T cell line using sgRNAs targeting either exon1 or exon2. Six clones with expected alterations at the TMEM70 genomic locus were retained for further analyses. They all showed undetectable levels of TMEM70 and marked reductions in the levels of several ATP synthase subunits whereas the CORE2 subunit of Complex III and the TOM20 subunit of the translocase of the outer mitochondrial membrane translocase were largely unaffected (Fig.3A).
Two clones, T3AA2 and T2BB9, were subjected to oxygen consumption assays in digitonin-permeabilized cells (Fig.3B). Three respiratory states were assessed: State 3 or phosphorylating state, in the presence of a saturating amount of ADP; Oligomycin state where ATP synthase is fully inhibited and the respiratory rate is minimal (compensates only the membrane passive permeability to protons); and the CCCP uncoupled state where respiratory rate is maximal in the absence of upstream kinetic control. State 3 respiration was decreased in both knock-out cell lines to a comparable extent when compared to wild-type HEK293T cells, whereas no significant difference between the mutant and control cells was observed in the oligomycin-inhibited and uncoupled states. Noteworthy, knock-out cells displayed an important 50-60% decrease in the ratio of state III over oligomycin state rates that indicates a specific ATP synthase deficiency (Fig.3C). As the characterized TMEM70 knock-out clones gave similar results, only one (T3AA2, hereafter designated as KO) was retained for all further experiments described below. We first investigated the assembly status and abundance of the ATP synthase in the KO cell line by probing ATPase activity in Blue Native gels, and the steady state levels of individual ATP synthase subunits by western

blot analysis of denaturing gels. Consistent with the respiration assays, these analyses revealed reduced amounts of assembled ATP synthase (Fig. 3D) and individual subunits in the KO cells (Fig. 3A) that were reversed to normal levels upon transduction with untagged or FLAG-tagged TMEM70 (Fig.3E). Interestingly, among the tested ATP synthase subunits, the content in Su.c was the most affected by the loss of expression of TMEM70, which is a unique feature among ATP synthase assembly-defective mutants (see introduction). In accordance with the bioenergetic demise and the role of the ATP synthase in shaping/maintaining cristae, mitochondrial ultrastructure was altered in the KO cells with less cristae and sometimes aberrant shape, and these defects were reversed upon restoration of TMEM70 expression (Fig.3F).

Investigation of TMEM70 stability and function in patient fibroblasts expressing mutant TMEM70 lacking the C-terminal hydrophilic domain of the protein

To confirm our observations in HEK293T cells subjected to silencing or knock-out of TMEM70, we analyzed cultured skin fibroblasts from a patient with a homozygous frame-shift mutation (c.497_498del) resulting in a truncation of TMEM70 after its second transmembrane segment (p.Tyr166Cysfs*7, Fig.4A). No signal for TMEM70 could be detected by western blot using the rabbit anti-peptides serum described above, indicating that the truncated protein was unstable and degraded (Fig.4A, Supp Fig.3). Several ATP synthase subunits were in strongly decreased amounts relative to control cells, such as the Su.c (Fig.4BC) and mitochondrial ultrastructure was altered with much less numerous and irregular arrangement of cristae and a matrix less dense to electrons (Fig.4D). All these alterations were efficiently suppressed upon transduction of the patient's fibroblasts with TMEM70 lentiviral construct. These results further corroborate the data obtained with KO cells and provide evidence that a compromised ability to assemble the ATP synthase was responsible for the disease of the patient with the c.497-498del mutation in TMEM70. They also underscore the importance of the C-terminal domain of TMEM70 for the stability of the protein, and hence for assembling the ATP synthase.

TMEM70 specifically protects subunit c from degradation regardless of other ATP synthase subunits and of the energetic status of mitochondria.

To gain further insights into the role of TMEM70 in ATP synthase assembly, we investigated the levels of ATP synthase subunits in cells endogenously expressing TMEM70 but devoid of mtDNA (Rho°) and thus missing core components of the respiratory chain and the two mtDNA-encoded Fo subunits Su.a and Su.A6L. We found that, similarly to TMEM70 KO cells, the levels of Su.c were significantly reduced compared to other ATP synthase subunits in Rho° cells (Fig. 5A). This observation raised the possibly that the lack in Su.c in TMEM70 KO cells was not primarily caused by the absence of TMEM70. However, we found that, similarly to Su.c, the levels of TMEM70 were also significantly reduced in Rho° cells (Fig. 5A). Interestingly, when the Rho° cells were transduced with our TMEM70 construct, normal steady state levels of Su.c were recovered (Fig.5B). Thus, the poor accumulation of Su.c in Rho° cells, while provoked by the loss of mtDNA (and mtDNA-encoded subunits), is likely caused by the loss of TMEM70 in these cells. Why the levels of TMEM70 are reduced in the absence of mtDNA is an interesting question that will deserve further investigation. However, the main result here is a reciprocal stabilization of Su.c and TMEM70.

Next, we aimed to know whether the F1 subcomplex, of nuclear genetic origin, also influences the stability of TMEM70. To this end, we knocked-down Su.Beta in rho$^+$ cells

(Fig.5C). While the Fo subunits b and d paralleled the depletion in F1 Su.Beta (indicating a major block in the assembly of the ATP synthase holoenzyme), the levels of Su.c, TMEM70, and a component of the respiratory complex I (NDUFB6) were not affected. The amounts of Su.c were reduced only when both TMEM70 and Su.Beta were knocked-down concomitantly (Fig.5C).

Taken together, these experiments revealed that TMEM70 is required to maintain the levels and stability of Su. c regardless of other ATP synthase subunits and of the energetic status of mitochondria. They further suggest that TMEM70 specifically protects subunit c from degradation indicating that the sharp reduction in fully assembled ATP synthase in cells lacking TMEM70 possibly results from a higher susceptibility to degradation of Su.c.

TMEM70 interacts transiently with subunit c before its incorporation into the ATP synthase

To gain further insights into the links between TMEM70 and Su.c, we investigated whether the two proteins could physically interact with each other. To this end, we isolated mitochondria from TMEM70 knock-out cells expressing untagged or FLAG-tagged TMEM70, solubilized mitochondria using digitonin (a mild detergent that preserves protein-protein interactions), and performed co-immunoprecipitation tests using TMEM70-FLAG as a bait. TMEM70-FLAG was almost entirely immunoprecipitated from the digitonin extracts using beads covalently bound to anti-FLAG monoclonal antibodies (Fig.6A). Su.c, but not other tested ATP synthase subunits, repeatedly co-immunoprecipitated with TMEM70-FLAG although in very small amounts. Noteworthy, in control experiments with non-tagged TMEM70, neither TMEM70 nor Su.c was pulled down. Since most Su.c was in the flow through, as other ATP synthase subunits (Fig. 6A: FT), we infer that TMEM70 transiently interacts with the low levels of Su.c not yet incorporated into the ATP synthase. Remarkably, similar results were also obtained with cells devoid of mtDNA (Supp Fig.4), indicating that mtDNA-encoded proteins, including Fo transmembrane subunits a and A6L, do not interact with TMEM70 and are not required for co-immunoprecipitation of TMEM70 and Su.c. An additional, weaker, immunological signal for TMEM70-FLAG was observed in our denaturing gels with approximately a doubled size suggesting that TMEM70 can form dimers, as previously reported (Hejzlarová *et al*, 2011; Kratochvílová *et al*, 2014), that are relatively resistant to detergents (Fig.6A). It is to be noted that untagged TMEM70 found in the flow-through of control experiments shows similar additional signal (considering the size of the tag), ruling out any artifact resulting from the tagged version. This result suggests that higher molecular weight complexes of TMEM70 would interact with Su.c.

In order to further define the interactions between TMEM70 and Su.c, we separated digitonin-solubilized protein complexes by two-dimensional electrophoresis (BlueNative/BN-PAGE followed by denaturing/SDS-PAGE) and analyzed them by western blot. In extracts from HEK293T control cells, as expected, ATP synthase subunits of the F1, proton channel, and peripheral stalk (Su.Beta, Su.c, Su.d, respectively) co-migrated at the position of fully assembled complex V (Fig.6B). Note that ATP synthase monomers and oligomers are not well resolved in this 4_16% polyacrylamide native gel. All TMEM70 signal was in smaller size complexes of grossly 300-400kDa (as compared to the calculated molecular weights of the F1 particle and free su.Beta detected with Su.Beta antibodies). This indicates that TMEM70 does not associate with fully assembled ATP synthase. Interestingly, in addition to the strong Su.c signal co-migrating with the ATP synthase, an additional Su.c signal of weaker intensity co-migrated with the protein complexes responding to TMEM70 antibodies. As expected, in

extracts from the TMEM70 KO clone (T3AA2) the Su.c signal exclusively co-migrated with Complex V (Fig. 6C). Consistent with the reduced amount of complex V in the KO cells, the antibodies against Su.Beta, Su.d and Su.c gave immunological signals of weaker intensities compared to the TMEM70-containing control samples. This confirmed that only Su.c yet unassembled into the ATP synthase interacts with TMEM70. Similar results were obtained with KO cell lines expressing either a FLAG-tagged version or an untagged version of TMEM70 (Fig.6DE). By contrast with the experiments shown in Fig.6BC, a 3-12% polyacrylamide native gel used here allowed ATP synthase monomers and oligomers to be well resolved. Interestingly, longer western blot exposures (Supp. Fig.5) revealed an additional weaker signal corresponding to TMEM70 dimers that we had observed in our immunoprecipitation assays.

To deepen our study, we then analyzed samples from the rho$^+$ cell line 143B and a Rho° derivative thereof both endogenously expressing TMEM70. With the rho$^+$ cells (Fig.6F), the results were similar to those obtained with wild-type HEK293T cells (Fig.6B) or with TMEM70 KO cells expressing exogenous TMEM70-FLAG or untagged TMEM70 (Fig.6DE). Consistent with previous studies (He *et al*, 2018, 2017b; Wittig *et al*, 2010), partial assemblies (also known as 'vestigial') containing all subunits except for the two mtDNA-encoded ones (a and A6L), DAPIT, and 6.8PL, could be identified in rho° cells that also accumulated F1 and F1-c subcomplexes that are barely detectable in rho$^+$ cells (Fig. 6FG). Interestingly the TMEM70-containing complexes and their co-migration with unassembled Su.c were still observed in the cells lacking mtDNA (Fig.6G). These data further show that none of the proteins encoded by mtDNA, notably Fo Su.a and Su.A6L, is involved in the interactions between TMEM70 and Su.c. This result provides additional evidence that TMEM70 interacts directly with Su.c. Furthermore, 2D analysis of immunoprecipitated TMEM-FLAG revealed that high molecular weight complexes resisting precipitation and elution depict several discrete spots of increasing molecular weights (Fig.6H). The existence of complexes with different TMEM70-Su.c stoichiometries points to gradual incorporation of c-subunits and suggests a role for TMEM70 oligomers in the gradual assembly of the c-ring (a homo-oligomeric ring of 8 Su.c molecules).

TMEM70 is specifically enriched in inner cristae membrane
The ATP synthase was shown, notably in mammals, to accumulate at the inner cristae membrane (ICM) where its oligomers are involved in the shaping of the membrane (Strauss *et al*, 2008; Davies *et al*, 2011; Jiko *et al*, 2015; Wilkens *et al*, 2013; Busch, 2020). An as-yet unresolved question is whether the biogenesis of the enzyme takes place at the inner boundary membrane (IBM) that faces the outer membrane, and then moves into the ICM, or whether assembly occurs within the ICM. Given the role of TMEM70 in ATP synthase biogenesis, we addressed this question by investigating TMEM70 localization within IBM and ICM using fluorescence microscopy. We first analyzed transduced cells expressing exogenous TMEM70 and compared its localization to that of Mitofilin/Mic60, a well characterized protein of the IBM that is a central component of the mitochondrial contact site and cristae organizing system (MICOS) localizing at cristae junctions (van der Laan *et al*, 2016). Standard confocal microscopy confirmed localization of both proteins within mitochondria but did not allow us to reveal their submitochondrial distribution (Fig.7A). Increasing the resolution by STED microscopy revealed a punctate pattern of both proteins throughout mitochondria. The Mic60 protein distributed to discrete punctae that appeared somewhat aligned at the mitochondria periphery, as previously described (Stoldt *et al*, 2019). In contrast, TMEM70

protein distributed to smaller dots with a more homogeneous distribution and no apparent enrichment in the mitochondrial periphery. To better discriminate between the two inner membrane domains, we developed an expansion microscopy approach. By opposition with STED that aims to increase optical resolution of the microscope, the rationale of expansion microscopy is rather to increase the size of the sample and image it with a standard wide-field microscope (Chozinski *et al*, 2016; Tillberg *et al*, 2016). In this way, the samples were expanded about four-fold in all three dimensions. To enable the parallel localization of TMEM70 and Mic60, we used cells stably expressing endogenous and FLAG-tagged TMEM70. (Fig. 7B). The localization of Mic60 to punctate MICOS structures at the mitochondrial periphery was confirmed. TMEM70-FLAG did not co-localize to Mic60-positive punctae, but distributed to structures entirely spanning the mitochondrial width as expected for mitochondrial cristae. Interestingly, the TMEM70-FLAG-labelled protrusions often aligned with Mic60, as expected from the localization of MICOS at the junctions between cristae and boundary membranes (See Fig.7D for a schematic representation). Finally, we localized endogenous TMEM70 with our TMEM70-specific antibodies. The signal to noise was lower, but the images depicted the cristae-like distribution observed for TMEM70-FLAG and no significant signal was observed in the inner boundary membrane (Fig.7C). These observations show that TMEM70 is mostly, if not exclusively, located within the inner cristae membrane (see Fig.7D), suggesting that the incorporation of subunit c, and possibly other steps of ATP synthase assembly, occur within the cristae domains of the inner mitochondrial membrane.

Discussion

Although a role for TMEM70 in mammalian ATP synthase biogenesis has been established in recent years (Braczynski *et al*, 2015; Cameron *et al*, 2011; Cízková *et al*, 2008; Jonckheere *et al*, 2011; Torraco *et al*, 2012; Vrbacký *et al*, 2016), its molecular function remained thus far poorly understood. We herein provide evidence that TMEM70 specifically interacts with Su.c before its assembly into the ATP synthase, protects Su.c from degradation, and facilitates its incorporation into the ATP synthase within cristae of the mitochondrial inner membrane.
In this study, we have confirmed that the lack of TMEM70 leads to a specific deficiency of the ATP synthase. In addition, we have shown that this is accompanied by a drastic drop in Su.c levels (see Fig. 2-4), which is a unique feature of TMEM70 deficiency and corroborates a very recent report (Kovalčíková *et al*, 2019). Whether the lack in Su.c was caused by a bioenergetic failure due to the compromised ability of the ATP synthase to assemble in the absence of TMEM70 and/or to the lack of another mitochondrial component(s) whose assembly/stability would be TMEM70-dependent was not known. We have resolved this issue (See Fig.5). First, we probed Su.c and TMEM70 in cells lacking mitochondrial DNA (rho°). Both proteins were in strongly reduced amounts in these cells but when TMEM70 was overexpressed a normal accumulation of Su.c was recovered. It can be inferred that any of the core subunits of complexes involved in the transfer of electrons to oxygen and of the two ATP synthase subunits encoded by the mtDNA, among which Su.a that is essential for Fo-mediated proton translocation, do not influence directly the stability of Su.c. We additionally show that the Su.c levels are not impacted when the F1-Beta protein was knocked down, similarly to cells in which one of the central stalk subunits of the F1 is silenced (Havlícková *et al*, 2010; Pecina *et al*, 2018). Moreover, Su.c levels were drastically reduced only when TMEM70 was concomitantly knocked-down. It can be concluded that

TMEM70 specifically controls the stability of Su.c within mitochondria before its incorporation into the ATP synthase, regardless of any other ATP synthase subunit and of the energetic status of mitochondria.

Recently, the presence of TMEM70 in pull down assays using a FLAG-version of su.c was reported (Kovalčíková *et al*, 2019), indicating the existence of possible interactions between Su.c and TMEM70. In these assays most of the Su.c pool was immunoprecipitated, which made it difficult to estimate the fraction of Su.c that interacts with TMEM70. Our immunoprecipitations of TMEM70 showed that only a minor amount of Su.c was pulled down, suggesting that TMEM70 possibly interacts only with subunits c not yet incorporated in the ATP synthase (Fig.6A). Further evidence for this is provided by the observation that TMEM70 takes part in 300-400 kDa protein complexes that do not co-migrate with ATP synthase holoenzyme, but only with a minor fraction of non-incorporated Su.c (Fig.6B-H). Consistently, no other subunit of ATP synthase was immunoprecipated using TMEM70 as a bait. In previous studies reporting the presence of TMEM70 in 550kDa and 470kD complexes (Torraco *et al*, 2012) it was argued that TMEM70 interacts with assembled ATP synthase whereas others failed to detect such interactions (Kratochvílová *et al*, 2014). The present study argues against an interaction of TMEM70 with ATP synthase complexes and provides evidence for the first time that TMEM70-containing complexes only make contacts with unassembled Su.c prior to its association with its protein partners within the ATP synthase.

Consistent with previous reports (Hejzlarová *et al*, 2011; Kratochvílová *et al*, 2014; Jonckheere *et al*, 2011), our biochemical studies localize endogenous TMEM70 in the mitochondrial inner membrane with the loop connecting its two transmembrane segments in the intermembrane space and the C-terminal hydrophilic domain on the other side of the membrane in the matrix (Fig.1). Interestingly, not only the hydrophilic C-terminal domain is evolutionary well conserved but the primary sequence of the transmembrane segments is particularly conserved (Supp Fig.6), indicating that they might not only represent membrane anchors. Possibly the transmembrane segments of TMEM70 interact with unassembled Su.c, not yet incorporated into ATP synthase. The ability of TMEM70 molecules to form dimers (Hejzlarová et al., 2011; Kratochvílová et al., 2014; this study) highly resistant even in denaturing conditions (Fig.6A and Supp. Fig.5), is an interesting property. Based on the molecular weight of TMEM70-containing complexes (Fig.6) and the known stoichiometry of eight Su.c within the c-ring, it is possible to envision the arrangement of eight TMEM70 dimers of 40 kDa in a complex of 320 KDa (Fig.8A). This octameric structure could interact with up to eight subunits c (380 KDa) and favor its assembly into an octameric c-ring (Fig.8A). We therefore propose that TMEM70 provides a scaffold easing the formation of the c-ring. In support to this hypothesis, the 2D analysis of our immunoprecipitates reveal a series of discrete TMEM70-Su.c complexes with apparent enrichment in Su.c content along with increasing molecular weight (Fig.6H). After completion of the c-ring and its incorporation into ATP synthase, the TMEM70 structure is released and can accommodate newly imported Su.c.

Applying expansion microscopy (Tillberg *et al*, 2016; Chozinski *et al*, 2016) to mitochondria provides evidence that TMEM70 localizes preferentially in cristae domains of the inner membrane (Fig. 7), as suggested by immunogold studies in an earlier report (Jonckheere *et al*, 2011). These observations suggest that formation of the Su.c-ring, which is considered an early step in the assembly process of ATP synthase, takes place within cristae as depicted in Fig. 8B rather than close to the MICOS-dependent contact sites between outer and inner membranes. A similar conclusion was reached in a recent study (Stoldt *et al*, 2018) in *S.*

cerevisiae, where in addition to Atp8 (yeast A6L) and Atp6 (yeast Su.a), the subunit c of the ATP synthase is encoded by the mitochondrial DNA. Indeed, factors specifically involved in the synthesis and assembly of these proteins were found preferentially located in cristae. On the opposite, the inner boundary membrane was found enriched in translation and assembly factors of yeast Complexes III and IV, indicating that the assembly of these two OXPHOS complexes preferentially start there and ongoing assembly intermediates are progressively moved into the cristae. These topographic differences in the biogenesis of OXPHOS complexes may contribute to the preferential accumulation of Complex V at the edge of cristae (Davies *et al*, 2011; Dudkina *et al*, 2010), which is presumably important for shaping the mitochondrial inner membrane (Paumard *et al*, 2002; Strauss *et al*, 2008). Consistently, mitochondrial ultrastructure was found perturbed in our TMEM70 KO cells and in cells from a patient carrying a premature stop codon after TM2 that destabilizes TMEM70 (Fig.3 and 4), similarly to tissues from a mouse lacking this protein (Vrbacký *et al*, 2016, 70) and other TMEM70 patients (Braczynski *et al*, 2015; Diodato *et al*, 2015; Cameron *et al*, 2011).

In yeast, Su.c would be synthesized in the vicinity of the inner membrane with the help of specific factors, including Aep1, Aep2 and the C-terminal half of Atp25 (Finnegan *et al*, 1991; Payne *et al*, 1993; Zeng *et al*, 2008), and inserted co-translationally into the membrane with the assistance of the protein translocase Oxa1 (Altamura *et al*, 1996; Jia *et al*, 2007). As a result, Su.c, which is an extremely hydrophobic protein referred to as a proteolipid, is protected from exposure and non-productive interactions in the aqueous mitochondrial matrix. With the relocation into the nucleus of its gene in mammals and a few other organisms including filamentous fungi (Anderson *et al*, 1981; De Grassi *et al*, 2006; Ridder *et al*, 1991), the sorting of Su.c to its final destination from the cytosol is more complex, and this has likely required specific adaptive evolution. For instance, evidence was provided that a functional allotopic expression of Su.c from the nucleus in yeast necessitates reducing the hydrophobicity of its first transmembrane segment presumably to avoid its lateral sorting in which case Su.c would be unable to reach a functional topology with its C- and N-termini in the intermembrane space (Bietenhader *et al*, 2012). Therefore, TMEM70 may be regarded as a factor whose emergence was required in mammals to take in charge Su.c after its transport into the organelle to protect it from degradation. The correlation between the levels of Su.c and TMEM70, regardless to the functional status of mitochondria and the presence of any other subunit of ATP synthase, strongly supports this hypothesis. However, other as-yet-unknown factors acting de concert with TMEM70 are certainly involved in the assembly pathway of mammalian Su.c, as evidenced by the down regulation of both Su.c and TMEM70 in cells lacking mtDNA.

The mitochondrial genome is a remnant of an ancestral prokaryotic genome that has considerably reduced in size during eukaryotic evolution due to a massive transfer of genes to the nucleus. To date, the main function of mitochondrial genomes is the production of a few subunits of the mitochondrial energy-transducing system. Some are always found in the mtDNA of respiring eukaryotes, like the ones encoding the cytochrome b subunit of Complex III and the Cox1 subunit of Complex IV; while others can be found in the nucleus or inside the organelle, like the gene encoding Su.c. The complexity of the functional relocation to the nucleus of this gene in yeast (Bietenhader *et al*, 2012) suggests that there must be some compelling reason to have it expressed from nuclear DNA. In support to this hypothesis, it was found that after its natural nuclear relocation in *Podospora anserina*, Su.c production and the efficacy of oxidative phosphorylation became highly regulated along the complex life cycle of this organism from two paralogous genes encoding structurally different

subunits c (Déquard-Chablat *et al*, 2011; Sellem *et al*, 2016). In humans where Su.c is also expressed from the nucleus, there are three Su.c gene isoforms, one of which (P1) shows transcriptional regulations in a cell- and tissue-specific manner, suggesting that as in filamentous fungi the Su.c became also a key regulatory target to modulate ATP production in humans. Studies by the group of J. Houstek have provided support to this hypothesis (Andersson *et al*, 1997; Houstek *et al*, 1995). On the other hand, important variations in the content of TMEM70 in mouse tissues have been reported recently (Kovalčíková *et al*, 2019). Therefore, the TMEM70-dependent assembly/stability of Su.c revealed in this study indicates that TMEM70 may play a key role in ATP synthase biogenesis modulation.

Materials and Methods

Cell lines and culture conditions

HEK293T were used throughout this study. 143B rho$^+$ (143B.TK-) is a human osteosarcoma-derived cell line (ATCC CRL 8303). 143B rho° (143B206) is an mtDNA-less derivative of 143B.TK- (King & Attardi, 1989). Both 143B derived cell lines were from Dr. Anne Chomyn (Caltech, USA). Primary human skin fibroblasts from a control individual and from a patient with cardiomyopathy carrying a homozygous frame-shift mutation c.497_498del in the TMEM70 gene were obtained from the Genetic unit of Necker-Enfants malades hospital (Paris, France) and were always kept at early passages. All cell lines were grown in Dulbecco's modified Eagle's medium (DMEM; Life Technologies) containing 4.5 g/l glucose, supplemented with 10% fetal bovine serum, 2 mM L-glutamine, 1 mM pyruvate, at 37°C under 5% CO_2. 50 μg/ml Uridine were added to this culture medium to grow 143B Rho+ and Rho° cell lines.

Plasmid constructs

TMEM70 cDNA was obtained by PCR amplification from HeLa cDNA preparation. Two fragments were amplified using the primers TMEM70-Fwd and TMEM70-noSfi-Rev or TMEM70-noSfi-Fwd and TMEM70-Rev-Stop in order to introduce a silent mutation (G>A) at position 141 of the coding sequence removing the internal *Sfi*I restriction site naturally present in TMEM70 coding sequence. The two fragments were fused by PCR to obtain a product corresponding to the 783 bp coding sequence of TMEM70 transcript variant 1 that was cloned into pMOS*blue* vector using the Blunt-Ended PCR Cloning Kit (GE Healthcare Life Sciences) to generate the pMOS-TMEM70 plasmid. The insert was subcloned into pKSPS (derived from pBluescriptIIKS(+) by inserting a *Sfi*I and *Pme*I sites in original *Kpn*I and *Sac*I sites, respectively) using the *Xho*I and *Eco*RI sites to generate the pKSPS-TMEM70 plasmid. As to generate a C-terminally FLAG-tagged version, the nucleotide sequence encoding the 3xFLAG epitope (DYKDDDDKDYKDDDDKDYKDDDDK) was obtained by annealing the two primers 3xFLAG-sense and 3xFLAG-antisense and cloned into the *Eco*RI and *Bam*HI sites of the pKSPS vector to generate the pKSPS-FLAG plasmid. TMEM70 cDNA was amplified by PCR from pKSPS-TMEM70 using a different primer at the 3' end (TMEM70-Rev-NoStop) removing the stop codon and the fragment obtained was cloned into the *Xho*I and *Eco*RI sites of pKSPS-FLAG, in frame with the 3xFLAG tag sequence, to generate pKSPS-TMEM70-FLAG. The TMEM70 and TMEM70-FLAG inserts were then subcloned into the previously described lentiviral vector pCMV-IRES-mitoDsRed (Frank *et al*, 2012) using the *Sfi*I and *Pme*I sites to generate the pCMV-TMEM70-IRES-mitoDsRed and pCMV-TMEM70_FLAG-IRES-mitoDsRed plasmids, respectively.

For TMEM70 knockdown studies, target sequences in TMEM70 mRNA were chosen (T1 GGGAAGGATATGTTCGATTCTTAAA and T2 CGAGTCTGATTGGCCTTACATTTCT) and primers were designed to encode shRNAs (shT1-Fwd/shT1-Rev and shT2-Fwd/shT2-Rev). For each construct, complementary primers were hybridized and cloned into the *Bam*HI and *Eco*RI sites of the lentiviral pSIH-H1-copGFP-shRNA vector (System Biosciences) according to the manufacturer's instructions to generate pSIH-T1 and pSIH-T2 plamsids for constitutive knockdown. In order to achieve doxycycline-inducible knockdown, a different set of primers targeting same regions of TMEM70 mRNA was used (shT1-Fwd-pLV, shT1-Rev-pLV, shT2-Fwd-pLV, shT2-Rev-pLV) to clone shRNA encoding sequences into the *Mlu*I and *Cla*I sites of the lentiviral pLVTHM vector (Wiznerowicz & Trono, 2003) in order to generate pLVTHM-T1

12

and pLVTHM-T2. pLVTHM and pLV-tTR-KRAB-red were gifts from Didier Trono (Addgene plasmids # 12247 and # 12250). To perform the Su.Beta knockdown, TRC2-pLKO-puro-shBeta3 (NM_001686.3-422s21c1) and TRC2-pLKO-puro-shBeta4 (NM_001686.3-1488s21c1) lentiviral constructs (Sigma-Aldrich) expressing shRNAs targeting the ATP5B mRNA were used.

To generate TMEM70 Knockout cell lines using the CRISPR-Cas9 technology, four different sgRNAs designed previously for a genome-scale CRISPR-Cas9 knockout (GeCKO) screening (Shalem *et al*, 2014) were used, two (TMEM70_sgRNA-1 and TMEM70_sgRNA-2) targeted to the first exon and two others (TMEM70_sgRNA-3 and TMEM70_sgRNA-4) targeted to the second exon of the TMEM70 gene. The dual vector GeCKO system was used consisting of plentiCas9-Blast and lentiGuide-Puro (Sanjana *et al*, 2014). For each construct, a pair of primers was hybridized and cloned into the BsmBI site of pLentiguide-Puro as described by the authors to generate the pLentiguide-Puro-TMEM70_sgRNA-1 to 4. plentiCas9-Blast and lentiGuide-Puro were gifts from Feng Zhang (Addgene # 52962 and # 52963 plasmids). The sequences of all primers used for these constructs can be found in Table 1.

Generation of TMEM70 KO cell lines by CRISPR-Cas9

HEK293T cells were co-transfected with pLentiCas9-Blast and either of the sgRNA constructs targeting the TMEM70 gene. 48 hours after transfection, the cells were passaged and subjected to antibiotic selection (Blasticidin 20 µg/ml and Puromycin 2 µg/ml) for three days. Cells were then allowed to recover and amplify without antibiotics for 5 days before samples were taken for analysis and frozen stocks of viable cells were prepared. sgRNA-2 and sgRNA-3 series were the most effective constructs, *i.e.* with minimal signal of TMEM70 protein by western blot. Corresponding cells were cultured again and cloned in 96 well-plates by critical dilution. A first screening by western blot allowed to select clones showing no expression of TMEM70 of which three from each series were selected (T2AC2/T2AC11/T2BB9 for sgRNA-2, and T3AA2/T3AG7/T3BH6 for sgRNA-3). For these clones, the exon (n°1 or 2) of TMEM70 targeted by the corresponding sgRNA was amplified by PCR using the primer pairs TMEM70Ex1-Fwd/TMEM70Ex1-Rev or TMEM70Ex2-Fwd/TMEM70Ex2-Rev, respectively, and sequenced in both directions using the same primers. The chromatograms were analyzed using the ICE algorithm (https://ice.synthego.com/#/) that revealed most CRISPR edits. When required, the PCR products were cloned into the pGEM-T vector (Promega). Sequencing of the inserts from a dozen of subclones in each case allowed us to ascertain the edits in TMEM70 exons. All edits were short deletions/insertions close to the expected cut site leading to frame-shifts and early stop codons.

Generation of stable cell lines

Lentiviral particles were generated in HEK293T cells according to (Zufferey *et al*, 1998). Cell lines were transduced with lentiviruses at a multiplicity of infection (MOI) of 1 unless otherwise specified and incubated for two to three days. Transduced cells were further amplified and either selected using antibiotic resistance (Su.Beta knockdown) or subjected to fluorescence assisted cell sorting (FACS) according to the fluorescent proteins co-expressed by the plasmids. For RNA interference studies the same rationale was used with additional peculiarities. In order to achieve doxycycline inducible TMEM70 knock-down, HEK293T cells were first transduced with lentiviruses bearing the pLV-tTR-KRAB-red construct at MOI 2 and were subjected to a second transduction with both the pLVTHM-T1 and pLVTHM-T2 constructs at MOI 5 each. shRNAs induction was triggered by addition of

doxycycline 250 ng/ml. Cells were cultured in the presence of doxycycline for various times with medium replacement every two to three days. To perform the Su.Beta knockdown, HEK293T were transduced with TRC2-pLKO-puro-shBeta3 and TRC2-pLKO-puro-shBeta4 lentiviral particles at MOI 3 each. For TMEM70 and Su.Beta double knock-down, the same cells were further transduced with pSIH-T1 and pSIH-T2 at MOI 3 each.

Primary Antibodies
Anti-TMEM70 antibodies were rabbit polyclonal sera raised by Eurogentec SA (Belgium) against a mixture of two peptides: an internal peptide located within the N-terminal part of the mature protein TPSDKSEDGRLIYTG and the C-terminal peptide YMEETSEEKRHKDDK, respectively P1 and P2 in Fig.1A. TMEM70 anti-sera were used at a 1:1000 dilution in western blots. Reactivity of sera against each peptide was validated by ELISA (See Supp. Fig. 1A). The following commercial primary antibodies were used throughout this study: Mouse monoclonal antibodies against Actin (clone C4 MAB1501R, Millipore), Fibrillarin (ab18380, Abcam), Cytochrome c (556433, BD Biosciences), VDAC1 (ab14734, Abcam), anti-FLAG M2 (F1804), Core2/UQCRC2 (ab14745, Abcam), NDUFB6 (ab110244, Abcam), SDHA (ab14715, Abcam), Su.Alpha/ATP5A (ab14748, Abcam), Su.Beta/ATPB (ab14730, Abcam), Su.d/ATP5H (ab110275, Abcam), Su.b/ATP5F1 (ab117991, Abcam), Su.OSCP/ATP5O (ab110276, Abcam); Rabbit Polyclonal antibodies against ERGIC p58 (E1031, Sigma), Mitofilin/Mic60 (10179-1-AP, Proteintech), TOM20 (SC-11415, Santa-Cruz); and Rabbit monoclonal antibodies against Su.c/ATP5G1/G2/G3 (ab180149, Abcam).

Subcellular fractionation
Cell fractionation protocol was adapted from previously established protocols (Duvezin-Caubet *et al*, 2006a). Cells were harvested, washed in PBS, resuspended in a HEPES 10 mM buffer at pH7.4 containing Mannitol 210 mM, Sucrose 70 mM, EDTA 1 mM, cOmplete^{TM} protease inhibitor cocktail (MB buffer) and homogenized on ice by several passages through a 25G needle fitted to a 2-5 ml syringe. All further steps were done at 4°C or on ice. The cell extract was first centrifuged at 700g for 10 min in order to pellet nuclei, cell debris, and unbroken cells. These steps were repeated until almost no unbroken cells were remaining in the pellet. Supernatants were further centrifuged at 1.000 g and all pellets were pooled in the nuclei enriched fraction. Supernatants from the last step were pooled and further centrifuged at 10.000 g for 10 min to pellet a fraction enriched in mitochondria (corresponding to the isolated mitochondria used throughout this study). Last supernatant was then subjected to ultracentrifugation at 130.000 g for 30 min in order to pellet a microsomal fraction and isolate a cytosolic fraction in the supernatant. Proteins from all factions were precipitated with trichloroacetic acid, centrifuged at 25.000 g for 10 min, washed with cold acetone, allowed to dry and solubilized in loading buffer.

Submitochondrial fractionation
Salt and carbonate extraction were adapted from previously established protocols (Duvezin-Caubet *et al*, 2006a). Briefly, isolated mitochondria were resuspended in HEPES-KOH 20 mM buffer supplemented with either KCl 500 mM at pH7.4 and sonicated 10 times for 10 seconds with 10 seconds breaks, or Na_2CO_3 0.1 M at pH11 and sonicated once 10 seconds and incubated for 30 min on ice. All samples were centrifuged for 10 min at 16.000 g. All supernatants and pellets were treated as described for cell fractions. For protease protection assay, isolated mitochondria were either resuspended in MB buffer or swollen by

resuspension in HEPES-KOH 20 mM pH7.4. For each buffer condition, two tubes were prepared among which one was supplemented with 200 µg/ml Proteinase K. After incubating for 30 min on ice, 2 mM PMSF were added to samples to inhibit the proteinase K and further incubated for 5 min on ice. All samples were centrifuged for 10 min at 16.000 g. Pellets were treated as described for cell fractions.

Total protein extracts
Cells were harvested, washed with PBS, resuspended in 10 volumes of RIPA buffer (Tris-HCl 50 mM pH8.0, 150 mM NaCl, 1% IGEPAL®CA-630, 0.5% sodium deoxycholate, 0.1% sodium dodecyl sulfate) supplemented with cOmplete™ protease inhibitor cocktail (Roche) and incubated for 20 minutes on ice. The suspensions were then centrifuged at 4°C for 20 minutes at 12000g and supernatants were transferred to fresh tubes. Protein concentrations were determined using the BCA assay kit (Pierce).

SDS-PAGE and western blot
Protein samples were lysed in loading buffer (Tris-HCl pH6.8 62.5 mM, Glycerol 10%, SDS 2%, bromophenol blue 0.002%, dithiothreitol 100 mM) and separated by SDS-PAGE using NuPAGE Bis-tris or Bolt Bis-Tris (12% or 4-12%) precast gels (Invitrogen) and MOPS or MES running buffers, respectively. Proteins were then transferred to nitrocellulose membrane in Tris 25 mM, Glycine 192 mM, 20% ethanol using a Mini Trans-Blot® cell (Bio-Rad), probed with desired primary antibodies in TBS-T buffer (Tris 20 mM pH8.0, NaCl 137 mM, 0.05% (w/v) Tween-20), supplemented with 5% (w/v) non-fat dry milk, revealed by chemiluminescence using peroxidase-conjugated Goat anti-Rabbit or Goat anti-Mouse IgG (H+L) secondary antibodies (Jackson ImmunoResearch) and Clarity™ western blot ECL substrate (BioRad). Signals were acquired using a G:BOX (Syngene) and quantified using the ImageJ software.

BN-PAGE of isolated mitochondria
BN-PAGE experiments were performed as described previously (Fronzes *et al*, 2006; Schagger *et al*, 1994) with some modifications. Mitochondria (300 µg mitochondrial proteins) were resuspended in 30 µl of 30 mM HEPES pH7.4, 150 mM potassium acetate, 12% (w/v) glycerol, 2 mM 6-aminocaproic acid, 1 mM EDTA, cOmplete^{TM} protease inhibitors (Roche), with digitonin (digitonin to protein ratio of 2 g/g), and incubated for 30 min at 4°c in a thermomixer (1400 rpm). Insoluble material was eliminated (pellet) by centrifugation at 4°C for 20 min at 25.000 g. 1µl of loading buffer (750 mM 6-aminocaproic acid 5% (w/v) Coomassie G-250) was added to the protein extract (supernatant) before loading on the gel. BN-PAGE was performed using NativePAGE 3-12% or 4-16% Bis-Tris gels and associated running buffer (Invitrogen). The cathode buffer was supplemented with 0.002% (w/v) Coomassie G-250. After electrophoresis, gels were either incubated in a solution of Lead acetate 0.5 g/L, ATP 4 mM, Glycine 270 mM, MgSO4 14 mM, Triton X-100 0.1%, Tris 35 mM pH8.4 to detect ATPase activity or subjected to two-dimensional SDS-PAGE.

Two-dimensional electrophoresis BN-PAGE/SDS-PAGE
To perform two-dimensional electrophoresis, we used 2D NuPAGE gels and adapted protocols from the manufacturer's instructions and previous reports (Lasserre *et al*, 2012, 2010). Individual lanes from the BN-PAGE were excised and first equilibrated for 5 min in Tris 50 mM pH8.5, urea 6M, glycerol 30%, SDS 2% at room temperature under gentle agitation,

then for 20 min in reducing conditions in the same buffer supplemented with DTT 100 mM, followed by a 20 min alkylation step in equilibration buffer containing iodoacetamide 135 mM, and a final 5 min washing step in 2D equilibration buffer. The gel lane was then transferred to a 2D well of a NuPAGE Bis-Tris 4-12% gradient gel. After the migration, the proteins were transferred to nitrocellulose as described for SDS-PAGE and analyzed by western blot.

Immunoprecipitation

Mitochondrial extracts were prepared exactly as described for BN-PAGE, then 10-fold diluted in TBS buffer (50mM Tris-HCl pH 7.5; 150mM NaCl) supplemented with cOmplete^{TM} protease inhibitors (Roche). ANTI-FLAG M2 Magnetic Beads (SIGMA) were prepared as described by the manufacturer, resuspended in the end in TBS, mixed with approximately equal volume of mitochondrial lysate, and incubated for 2 hours at room temperature in an end over end shaker. The supernatant (flow-through) was aspirated and the beads were then washed three times with TBS buffer supplemented with 0,1% digitonin and eluted by competition with 150µg/ml 3xFLAG peptide (Sigma) in TBS + 0,1% digitonin for 30 minutes at 4°C in an end over end shaker.

Immunofluorescence of human cells.

Human skin fibroblasts or 143B cells expressing TMEM70-FLAG were seeded at a density of ~100,000 cells per well in a six-well plate containing 12-mm coverslips and incubated overnight. Cells were fixed with 4% paraformaldehyde (PFA) in PBS for 20 min. After fixation, cells were quickly washed 3 times in PBS and post-extracted for 10 min in PBS with 0.1% Triton X-100. PFA free radicals in excess were reduced with 10 mM NH_4Cl in PBS for 10 min, then cells were incubated in the blocking buffer (BF; PBS with 1% BSA) for 15 min. Next, coverslips were incubated with primary antibody diluted in the BF for 1h at 37°C. Coverslips were then washed in BF three times for 5 min and subsequently incubated for 45 min at 37°C with secondary antibody diluted in BF in dark chamber. Finally, coverslips were washed in PBS three times for 5 min, and mounted on a glass slide with ProlonGold® mounting medium. For immunolabeling, primary antibodies were rabbit polyclonal anti-TMEM70 (1:100), rabbit polyclonal anti-MIC60 (1:200), mouse monoclonal anti-FLAG (1:500); and secondary antibodies were goat anti-mouse Alexa 647 IgG (H+L), goat anti-rabbit Alexa 568 IgG (H+L) (1:100; Invitrogen), goat anti-mouse Atto 647N (1:100; Sigma-Aldrich), or anti-rabbit STAR-580 and anti-mouse STAR-RED (1:200; Abberior) for STED acquisition. For Expansion microscopy, after the last PBS wash of standard immunofluorescence, cells were proceeded exactly as described by (Chozinski *et al*, 2016).

Optical Microscopy

Expanded cells were imaged with a UPlanSApo 100×/1.4 oil immersion objective in an Olympus IX81 microscope (Olympus, Tokyo, Japan). Z-stacks were deconvolved using the DeconvolutionLab plugin. Stimulated Emission Depletion (STED) imaging was performed using a STEDYCON (Abberior Instruments GmbH, Göttingen) with excitation lasers at 488, 561, and 640 nm, and a STED laser at 775 nm (maximum intensity 1.25 W; all lasers are pulsed with 40 MHz repetition rate). The STEDYCON was mounted on the camera port of an AxioImager Z2 upright microscope (Zeiss, Jena, Germany), equipped with a 100x objective (alpha Plan-Apochromat, Oil, DIC, Vis, NA 1.46; Zeiss). The pinhole was set to 1.1 Airy units for 650 nm emission. Fluorescence was detected on avalanche photo diodes, with emission

bands between 650–700 nm, 578–627 nm, and 505–545 nm, respectively. Data was stored in .obf format and exported as tif files for further analysis.

Electron microscopy

Cells were fixed for 45 min at 4°C in 4% PFA in PBS, washed and fixed again for 1 h at room temperature in 2% osmium tetroxide in PBS containing 15 mg/ml of $K_4Fe(CN)_6$. Dehydration was performed with ethanol series (50%, 70%, 95% and absolute ethanol). Thereafter, the samples were embedded progressively in Epon resin. Ultrathin sections were contrasted with 1% lead citrate in water for 1 min. Sample imaging was performed using a Hitachi H7650 transmission microscope operated at 80 KV with a Gatan—11 MPx camera at electron microscopy unit (Bordeaux imaging center).

Oxygen consumption measurements

Cells from around 60% confluent Petri dishes were detached using trypsin, harvested by centrifugation at 1.000g for 8 min at 4°C and resuspended in 100 μl PBS. Oxygen consumption rates were measured with 1.10^6 cells/ml by high resolution respirometry in an Oxygraph-2k (Oroboros Instruments) in respiration buffer (sucrose 120 mM, KCl 50 mM, KH_2PO_4 4 mM, $MgCl_2$ 2 mM, EGTA 1 mM, Tris-HCl 20 mM pH7.2) supplemented subsequently with succinate 5 mM, ADP 2.5 mM, oligomycin 2 μg/ml, and CCCP 0.25 μM.

Acknowledgements

Author contributions

SDC, AD, and JPdR, and ET conceived the study. HB, JB, and SDC designed and conducted the majority of experiments and analyzed the data. JD and MR designed and performed immunofluorescence microscopy experiments and data analysis. BS and CB performed electron microscopy experiments and data analysis. MRose designed, performed and analyzed part of knockdown and 2D experiments. SC provided technical support in CRISPR/Cas9 experiments. SDC and ABAE supervised the project. SDC wrote the original draft and reviewed and edited the manuscript together with AD, JPdR, MR, and ET. All authors approved the final version of the manuscript.

Conflict of interest

The authors declare that they have no conflict of interest.

References

Altamura N, Capitanio N, Bonnefoy N, Papa S & Dujardin G (1996) The Saccharomyces cerevisiae OXA1 gene is required for the correct assembly of cytochrome c oxidase and oligomycin-sensitive ATP synthase. *FEBS Lett.* **382:** 111–115

Anderson S, Bankier AT, Barrell BG, de Bruijn MH, Coulson AR, Drouin J, Eperon IC, Nierlich DP, Roe BA, Sanger F, Schreier PH, Smith AJ, Staden R & Young IG (1981) Sequence and organization of the human mitochondrial genome. *Nature* **290:** 457–465

Andersson U, Houstek J & Cannon B (1997) ATP synthase subunit c expression: physiological regulation of the P1 and P2 genes. *Biochem. J.* **323:** 379–385

Bietenhader M, Martos A, Tetaud E, Aiyar RS, Sellem CH, Kucharczyk R, Clauder-Münster S, Giraud M-F, Godard F, Salin B, Sagot I, Gagneur J, Déquard-Chablat M, Contamine V, Denmat SH-L, Sainsard-Chanet A, Steinmetz LM & Rago J-P di (2012) Experimental Relocation of the Mitochondrial ATP9 Gene to the Nucleus Reveals Forces Underlying Mitochondrial Genome Evolution. *PLOS Genet.* **8:** e1002876

Braczynski AK, Vlaho S, Müller K, Wittig I, Blank A-E, Tews DS, Drott U, Kleinle S, Abicht A, Horvath R, Plate KH, Stenzel W, Goebel HH, Schulze A, Harter PN, Kieslich M & Mittelbronn M (2015) ATP synthase deficiency due to TMEM70 mutation leads to ultrastructural mitochondrial degeneration and is amenable to treatment. *BioMed Res. Int.* **2015:** 462592

Busch KB (2020) Inner mitochondrial membrane compartmentalization: Dynamics across scales. *Int. J. Biochem. Cell Biol.* **120:** 105694

Cameron JM, Levandovskiy V, Mackay N, Ackerley C, Chitayat D, Raiman J, Halliday WH, Schulze A & Robinson BH (2011) Complex V TMEM70 deficiency results in mitochondrial nucleoid disorganization. *Mitochondrion* **11:** 191–199

Carrozzo R, Wittig I, Santorelli FM, Bertini E, Hofmann S, Brandt U & Schägger H (2006) Subcomplexes of human ATP synthase mark mitochondrial biosynthesis disorders. *Ann. Neurol.* **59:** 265–275

Chozinski TJ, Halpern AR, Okawa H, Kim H-J, Tremel GJ, Wong ROL & Vaughan JC (2016) Expansion microscopy with conventional antibodies and fluorescent proteins. *Nat. Methods* **13:** 485–488

Cízková A, Stránecký V, Mayr JA, Tesarová M, Havlícková V, Paul J, Ivánek R, Kuss AW, Hansíková H, Kaplanová V, Vrbacký M, Hartmannová H, Nosková L, Honzík T, Drahota Z, Magner M, Hejzlarová K, Sperl W, Zeman J, Houstek J, et al (2008) TMEM70 mutations cause isolated ATP synthase deficiency and neonatal mitochondrial encephalocardiomyopathy. *Nat. Genet.* **40:** 1288–1290

Davies KM, Strauss M, Daum B, Kief JH, Osiewacz HD, Rycovska A, Zickermann V & Kühlbrandt W (2011) Macromolecular organization of ATP synthase and complex I in whole mitochondria. *Proc. Natl. Acad. Sci. U. S. A.* **108:** 14121–14126

De Grassi A, Lanave C & Saccone C (2006) Evolution of ATP synthase subunit c and cytochrome c gene families in selected Metazoan classes. *Gene* **371:** 224–233

De Meirleir L, Seneca S, Lissens W, De Clercq I, Eyskens F, Gerlo E, Smet J & Van Coster R (2004) Respiratory chain complex V deficiency due to a mutation in the assembly gene ATP12. *J. Med. Genet.* **41:** 120–124

Déquard-Chablat M, Sellem CH, Golik P, Bidard F, Martos A, Bietenhader M, di Rago J-P, Sainsard-Chanet A, Hermann-Le Denmat S & Contamine V (2011) Two Nuclear Life Cycle–Regulated Genes Encode Interchangeable Subunits c of Mitochondrial ATP Synthase in Podospora anserina. *Mol. Biol. Evol.* **28:** 2063–2075

Diodato D, Invernizzi F, Lamantea E, Fagiolari G, Parini R, Menni F, Parenti G, Bollani L, Pasquini E, Donati MA, Cassandrini D, Santorelli FM, Haack TB, Prokisch H, Ghezzi D, Lamperti C & Zeviani M (2015) Common and Novel TMEM70 Mutations in a Cohort of Italian Patients with Mitochondrial Encephalocardiomyopathy. *JIMD Rep.* **15:** 71–78

Dudkina NV, Oostergetel GT, Lewejohann D, Braun H-P & Boekema EJ (2010) Row-like organization of ATP synthase in intact mitochondria determined by cryo-electron tomography. *Biochim. Biophys. Acta* **1797:** 272–277

Duvezin-Caubet S, Caron M, Giraud M-F, Velours J & di Rago J-P (2003) The two rotor components of yeast mitochondrial ATP synthase are mechanically coupled by subunit delta. *Proc. Natl. Acad. Sci. U. S. A.* **100:** 13235–13240

Duvezin-Caubet S, Jagasia R, Wagener J, Hofmann S, Trifunovic A, Hansson A, Chomyn A, Bauer MF, Attardi G, Larsson N-G, Neupert W & Reichert AS (2006a) Proteolytic processing of OPA1 links mitochondrial dysfunction to alterations in mitochondrial morphology. *J. Biol. Chem.* **281:** 37972–37979

Duvezin-Caubet S, Rak M, Lefebvre-Legendre L, Tetaud E, Bonnefoy N & di Rago J-P (2006b) A 'petite obligate' mutant of Saccharomyces cerevisiae: functional mtDNA is lethal in cells lacking the delta subunit of mitochondrial F1-ATPase. *J. Biol. Chem.* **281:** 16305–16313

Fearnley IM & Walker JE (1986) Two overlapping genes in bovine mitochondrial DNA encode membrane components of ATP synthase. *EMBO J.* **5:** 2003–2008

Finnegan PM, Payne MJ, Keramidaris E & Lukins HB (1991) Characterization of a yeast nuclear gene, AEP2, required for accumulation of mitochondrial mRNA encoding subunit 9 of the ATP synthase. *Curr. Genet.* **20:** 53–61

Frank M, Duvezin-Caubet S, Koob S, Occhipinti A, Jagasia R, Petcherski A, Ruonala MO, Priault M, Salin B & Reichert AS (2012) Mitophagy is triggered by mild oxidative stress in a mitochondrial fission dependent manner. *Biochim. Biophys. Acta* **1823:** 2297–2310

Fronzes R, Weimann T, Vaillier J, Velours J & Brèthes D (2006) The Peripheral Stalk Participates in the Yeast ATP Synthase Dimerization Independently of e and g Subunits. *Biochemistry* **45:** 6715–6723

Fujikawa M, Sugawara K, Tanabe T & Yoshida M (2015) Assembly of human mitochondrial ATP synthase through two separate intermediates, F1-c-ring andb–e–g complex. *FEBS Lett.* **589:** 2707–2712

Fukasawa Y, Tsuji J, Fu S-C, Tomii K, Horton P & Imai K (2015) MitoFates: improved prediction of mitochondrial targeting sequences and their cleavage sites. *Mol. Cell. Proteomics MCP* **14:** 1113–1126

Habersetzer J, Larrieu I, Priault M, Salin B, Rossignol R, Brèthes D & Paumard P (2013) Human F1F0 ATP synthase, mitochondrial ultrastructure and OXPHOS impairment: a (super-)complex matter? *PloS One* **8:** e75429

Havlícková V, Kaplanová V, Nůsková H, Drahota Z & Houstek J (2010) Knockdown of F1 epsilon subunit decreases mitochondrial content of ATP synthase and leads to accumulation of subunit c. *Biochim. Biophys. Acta* **1797:** 1124–1129

He J, Carroll J, Ding S, Fearnley IM & Walker JE (2017a) Permeability transition in human mitochondria persists in the absence of peripheral stalk subunits of ATP synthase. *Proc. Natl. Acad. Sci.* **114:** 9086–9091

He J, Ford HC, Carroll J, Ding S, Fearnley IM & Walker JE (2017b) Persistence of the mitochondrial permeability transition in the absence of subunit c of human ATP synthase. *Proc. Natl. Acad. Sci.* **114:** 3409–3414

He J, Ford HC, Carroll J, Douglas C, Gonzales E, Ding S, Fearnley IM & Walker JE (2018) Assembly of the membrane domain of ATP synthase in human mitochondria. *Proc. Natl. Acad. Sci.* **115:** 2988–2993

Hejzlarová K, Tesařová M, Vrbacká-Čížková A, Vrbacký M, Hartmannová H, Kaplanová V, Nosková L, Kratochvílová H, Buzková J, Havlíčková V, Zeman J, Kmoch S & Houštěk J (2011) Expression and processing of the TMEM70 protein. *Biochim. Biophys. Acta* **1807:** 144–149

Houstek J, Andersson U, Tvrdík P, Nedergaard J & Cannon B (1995) The Expression of Subunit c Correlates with and Thus May Limit the Biosynthesis of the Mitochondrial F0F1-ATPase in Brown Adipose Tissue. *J. Biol. Chem.* **270:** 7689–7694

Jia L, Dienhart MK & Stuart RA (2007) Oxa1 directly interacts with Atp9 and mediates its assembly into the mitochondrial F1Fo-ATP synthase complex. *Mol. Biol. Cell* **18:** 1897–1908

Jiko C, Davies KM, Shinzawa-Itoh K, Tani K, Maeda S, Mills DJ, Tsukihara T, Fujiyoshi Y, Kühlbrandt W & Gerle C (2015) Bovine F1Fo ATP synthase monomers bend the lipid bilayer in 2D membrane crystals. *eLife* **4:** e06119

Jonckheere AI, Huigsloot M, Lammens M, Jansen J, van den Heuvel LP, Spiekerkoetter U, von Kleist-Retzow J-C, Forkink M, Koopman WJH, Szklarczyk R, Huynen MA, Fransen JA, Smeitink JAM & Rodenburg RJT (2011) Restoration of complex V deficiency caused by a novel deletion in the human TMEM70 gene normalizes mitochondrial morphology. *Mitochondrion* **11:** 954–963

Jonckheere AI, Renkema GH, Bras M, van den Heuvel LP, Hoischen A, Gilissen C, Nabuurs SB, Huynen MA, de Vries MC, Smeitink JAM & Rodenburg RJT (2013) A complex V ATP5A1 defect causes fatal neonatal mitochondrial encephalopathy. *Brain* **136:** 1544–1554

Jonckheere AI, Smeitink JAM & Rodenburg RJT (2012) Mitochondrial ATP synthase: architecture, function and pathology. *J. Inherit. Metab. Dis.* **35:** 211–225

Käll L, Krogh A & Sonnhammer ELL (2007) Advantages of combined transmembrane topology and signal peptide prediction--the Phobius web server. *Nucleic Acids Res.* **35:** W429-432

King MP & Attardi G (1989) Human cells lacking mtDNA: repopulation with exogenous mitochondria by complementation. *Science* **246:** 500–503

Kovalčíková J, Vrbacký M, Pecina P, Tauchmannová K, Nůsková H, Kaplanová V, Brázdová A, Alán L, Eliáš J, Čunátová K, Kořínek V, Sedlacek R, Mráček T & Houštěk J (2019) TMEM70 facilitates biogenesis of mammalian ATP synthase by promoting subunit c incorporation into the rotor structure of the enzyme. *FASEB J. Off. Publ. Fed. Am. Soc. Exp. Biol.* **33:** 14103–14117

Kratochvílová H, Hejzlarová K, Vrbacký M, Mráček T, Karbanová V, Tesařová M, Gombitová A, Cmarko D, Wittig I, Zeman J & Houštěk J (2014) Mitochondrial membrane assembly of TMEM70 protein. *Mitochondrion* **15:** 1–9

Krogh A, Larsson B, von Heijne G & Sonnhammer EL (2001) Predicting transmembrane protein topology with a hidden Markov model: application to complete genomes. *J. Mol. Biol.* **305:** 567–580

Kucharczyk R, Zick M, Bietenhader M, Rak M, Couplan E, Blondel M, Caubet S-D & di Rago J-P (2009) Mitochondrial ATP synthase disorders: molecular mechanisms and the quest for curative therapeutic approaches. *Biochim. Biophys. Acta* **1793:** 186–199

van der Laan M, Horvath SE & Pfanner N (2016) Mitochondrial contact site and cristae organizing system. *Curr. Opin. Cell Biol.* **41:** 33–42

Lasserre J-P, Fack F, Serchi T, Revets D, Planchon S, Renaut J, Hoffmann L, Gutleb AC, Muller CP & Bohn T (2012) Atrazine and PCB 153 and their effects on the proteome of subcellular fractions of human MCF-7 cells. *Biochim. Biophys. Acta BBA - Proteins Proteomics* **1824:** 833–841

Lasserre J-P, Nicaud J-M, Pagot Y, Joubert-Caron R, Caron M & Hardouin J (2010) First complexomic study of alkane-binding protein complexes in the yeast Yarrowia lipolytica. *Talanta* **80:** 1576–1585

Magner M, Dvorakova V, Tesarova M, Mazurova S, Hansikova H, Zahorec M, Brennerova K, Bzduch V, Spiegel R, Horovitz Y, Mandel H, Eminoğlu FT, Mayr JA, Koch J, Martinelli D, Bertini E, Konstantopoulou V, Smet J, Rahman S, Broomfield A, et al (2015) TMEM70 deficiency: long-term outcome of 48 patients. *J. Inherit. Metab. Dis.* **38:** 417–426

Mitchell P (1961) Coupling of phosphorylation to electron and hydrogen transfer by a chemi-osmotic type of mechanism. *Nature* **191:** 144–148

Nijtmans LG, Klement P, Houstěk J & van den Bogert C (1995) Assembly of mitochondrial ATP synthase in cultured human cells: implications for mitochondrial diseases. *Biochim. Biophys. Acta* **1272:** 190–198

Paumard P, Vaillier J, Coulary B, Schaeffer J, Soubannier V, Mueller DM, Brèthes D, di Rago J-P & Velours J (2002) The ATP synthase is involved in generating mitochondrial cristae morphology. *EMBO J.* **21:** 221–230

Payne MJ, Finnegan PM, Smooker PM & Lukins HB (1993) Characterization of a second nuclear gene, AEP1, required for expression of the mitochondrial OLI1 gene in Saccharomyces cerevisiae. *Curr. Genet.* **24:** 126–135

Pecina P, Nůsková H, Karbanová V, Kaplanová V, Mráček T & Houštěk J (2018) Role of the mitochondrial ATP synthase central stalk subunits γ and δ in the activity and assembly of the mammalian enzyme. *Biochim. Biophys. Acta BBA - Bioenerg.* **1859:** 374–381

Rak M, McStay GP, Fujikawa M, Yoshida M, Manfredi G & Tzagoloff A (2011) Turnover of ATP synthase subunits in F1-depleted HeLa and yeast cells. *FEBS Lett.* **585:** 2582–2586

Rak M, Zeng X, Brière J-J & Tzagoloff A (2009) Assembly of F0 in Saccharomyces cerevisiae. *Biochim. Biophys. Acta* **1793:** 108–116

Ridder R, Künkele K-P & Osiewacz HD (1991) Sequence of the nuclear ATP synthase subunit 9 gene of Podospora anserina: lack of similarity to the mitochondrial genome. *Curr. Genet.* **20:** 349–351

Sanjana NE, Shalem O & Zhang F (2014) Improved vectors and genome-wide libraries for CRISPR screening. *Nat. Methods* **11:** 783–784

Schagger H, Cramer WA & Vonjagow G (1994) Analysis of Molecular Masses and Oligomeric States of Protein Complexes by Blue Native Electrophoresis and Isolation of Membrane Protein Complexes by Two-Dimensional Native Electrophoresis. *Anal. Biochem.* **217:** 220–230

Sellem CH, di Rago J-P, Lasserre J-P, Ackerman SH & Sainsard-Chanet A (2016) Regulation of Aerobic Energy Metabolism in Podospora anserina by Two Paralogous Genes

Encoding Structurally Different c-Subunits of ATP Synthase. *PLoS Genet.* **12:** e1006161

Shalem O, Sanjana NE, Hartenian E, Shi X, Scott DA, Mikkelson T, Heckl D, Ebert BL, Root DE, Doench JG & Zhang F (2014) Genome-scale CRISPR-Cas9 knockout screening in human cells. *Science* **343:** 84–87

Stoldt S, Stephan T, Jans DC, Brüser C, Lange F, Keller-Findeisen J, Riedel D, Hell SW & Jakobs S (2019) Mic60 exhibits a coordinated clustered distribution along and across yeast and mammalian mitochondria. *Proc. Natl. Acad. Sci. U. S. A.* **116:** 9853–9858

Stoldt S, Wenzel D, Kehrein K, Riedel D, Ott M & Jakobs S (2018) Spatial orchestration of mitochondrial translation and OXPHOS complex assembly. *Nat. Cell Biol.* **20:** 528–534

Strauss M, Hofhaus G, Schröder RR & Kühlbrandt W (2008) Dimer ribbons of ATP synthase shape the inner mitochondrial membrane. *EMBO J.* **27:** 1154–1160

Tillberg PW, Chen F, Piatkevich KD, Zhao Y, Yu C-CJ, English BP, Gao L, Martorell A, Suk H-J, Yoshida F, DeGennaro EM, Roossien DH, Gong G, Seneviratne U, Tannenbaum SR, Desimone R, Cai D & Boyden ES (2016) Protein-retention expansion microscopy of cells and tissues labeled using standard fluorescent proteins and antibodies. *Nat. Biotechnol.* **34:** 987–992

Torraco A, Verrigni D, Rizza T, Meschini MC, Vazquez-Memije ME, Martinelli D, Bianchi M, Piemonte F, Dionisi-Vici C, Santorelli FM, Bertini E & Carrozzo R (2012) TMEM70: a mutational hot spot in nuclear ATP synthase deficiency with a pivotal role in complex V biogenesis. *Neurogenetics* **13:** 375–386

Vazquez-Calvo C, Suhm T, Büttner S & Ott M (2020) The basic machineries for mitochondrial protein quality control. *Mitochondrion* **50:** 121–131

Voos W (2013) Chaperone–protease networks in mitochondrial protein homeostasis. *Biochim. Biophys. Acta BBA - Mol. Cell Res.* **1833:** 388–399

Vrbacký M, Kovalčíková J, Chawengsaksophak K, Beck IM, Mráček T, Nůsková H, Sedmera D, Papoušek F, Kolář F, Sobol M, Hozák P, Sedlacek R & Houštěk J (2016) Knockout of Tmem70 alters biogenesis of ATP synthase and leads to embryonal lethality in mice. *Hum. Mol. Genet.*

Walker JE (2013) The ATP synthase: the understood, the uncertain and the unknown. *Biochem. Soc. Trans.* **41:** 1–16

Wang ZG, White PS & Ackerman SH (2001) Atp11p and Atp12p are assembly factors for the F(1)-ATPase in human mitochondria. *J. Biol. Chem.* **276:** 30773–30778

Wilkens V, Kohl W & Busch K (2013) Restricted diffusion of OXPHOS complexes in dynamic mitochondria delays their exchange between cristae and engenders a transitory mosaic distribution. *J Cell Sci* **126:** 103–116

Wittig I, Meyer B, Heide H, Steger M, Bleier L, Wumaier Z, Karas M & Schägger H (2010) Assembly and oligomerization of human ATP synthase lacking mitochondrial subunits a and A6L. *Biochim. Biophys. Acta* **1797:** 1004–1011

Wiznerowicz M & Trono D (2003) Conditional suppression of cellular genes: lentivirus vector-mediated drug-inducible RNA interference. *J. Virol.* **77:** 8957–8961

Zeng X, Barros MH, Shulman T & Tzagoloff A (2008) ATP25, a new nuclear gene of Saccharomyces cerevisiae required for expression and assembly of the Atp9p subunit of mitochondrial ATPase. *Mol. Biol. Cell* **19:** 1366–1377

Zufferey R, Dull T, Mandel RJ, Bukovsky A, Quiroz D, Naldini L & Trono D (1998) Self-Inactivating Lentivirus Vector for Safe and Efficient In Vivo Gene Delivery. *J. Virol.* **72:** 9873–9880

Figure legends

Figure 1. *Subcellular localization of TMEM70.* **A.** Scheme representing the domain organization of TMEM70 with amino-acid residues numbering above. MTS: Mitochondrial Targeting Sequence. TM: Transmembrane segment. Positions of immunogenic peptides are indicated (P1, P2). **B.** 143B-rho$^+$ cells were fractionated by differential centrifugation as detailed in the materials and methods section. Fractions enriched in nuclei (Nuc), mitochondria (Mito), microsomes (Micro), and cytosol were analyzed by SDS-PAGE and western blot using antibodies against indicated proteins. **C.** Isolated mitochondria from 143B-rho$^+$ cells were subjected to carbonate (Na2CO3 pH11.5) or salt (KCl 500 mM) extraction. Proteins from supernatants (Sup) and pellets were separated by SDS-PAGE and analyzed by western blot. **D.** Isolated mitochondria from 143B-rho$^+$ cells were subjected to a protease protection assay. Mitochondria were resuspended in hypotonic (Swelling +) or iso-osmotic buffer (Swelling -) in the presence (+PK) or absence (-PK) of Proteinase K. Protein pellets were separated by SDS-PAGE and analyzed by western blot. **E.** Topological model of TMEM70 within mitochondria. (IM) inner membrane; (IMS) intermembrane space. N- and C-termini of TMEM70 are indicated.

Figure 2. *Inducible knockdown of TMEM70.* HEK293T cells were transduced with constructs allowing the doxycycline-inducible expression of a mix of two shRNAs targeted to TMEM70 mRNA. **A.** Cells were cultured in the presence of doxycycline for the indicated time periods and harvested. Total protein extracts were separated by SDS-PAGE and analyzed by western blot. Representative signals obtained are shown in the inset. Signal densities were quantified and expressed as percentage of signal obtained in the absence of doxycycline. **B-D.** Cells were cultured in the presence of doxycycline for indicated time periods or left without the drug during equal time and harvested. Mitochondria were isolated from the cell pellets and analyzed as follows. **B.** Mitochondria were lysed, and proteins were separated by SDS-PAGE and analyzed by western blot. **C.** Quantitation of signal intensities from B. Signals were normalized to VDAC1 used as a loading control. For each protein tested, an average of normalized signals in the presence of doxycycline at the different time points is shown as a percentage of the average signal obtained in the absence of doxycycline; +/- Standard Deviation. **D.** Digitonin extracts from the isolated mitochondria were subjected to CN-PAGE and ATPase activity was revealed in-gel (white precipitate). The position of ATP synthase monomers (M) and dimers (D) are indicated to the right. The relative positions of molecular weight markers are indicated to the left. **E.** Scheme of the human ATP synthase structure. The general structure of the complex is represented on the scheme with the different types of subunits colored and named.

Figure 3. *Characterization of TMEM70-knockout cells generated from HEK293T.* **A.** Isolated mitochondria from different TMEM70-KO clones and HEK293T as a control were lysed and proteins were separated by SDS-PAGE and analyzed by western blot. The faint signal indicated by * just below TMEM70 band is an unspecific cross-reaction of anti-TMEM70 serum. **B.** TMEM70-KO (T3AA2; T2BB9) and HEK293T permeabilized cells were subjected to oxygen consumption measurements after addition of ADP, Oligomycin, and CCCP. The results shown, expressed in nmolO$_2$/min/10^6cells, are average +/- SD of 6 to 9 measurements from 3 to 4 biological replicates, respectively.

C. The ratio of ADP-stimulated rate over Oligomycin-inhibited rate was calculated for each measurement and the average ratios +/- SD for each cell line are represented in the bar graph with corresponding numerical values indicated above each bar. **D.** Digitonin extracts from Isolated mitochondria of wild-type (HEK293T), T3AA2 TMEM70 knock-out (KO), and the same KO cell line expressing exogenous TMEM70 (KO+TMEM70) were subjected to BN-PAGE and ATPase activity was revealed in-gel (white precipitate). ATP synthase monomers (M) and dimers (D) are detected in these conditions. **E.** Isolated mitochondria from KO cell lines transduced with the indicated constructs were lysed and proteins were separated by SDS-PAGE and analyzed by western blot. **F.** TMEM70 KO cells expressing TMEM70 cDNA (KO + TMEM70) or not (KO) were fixed, sliced and imaged by transmission electron microscopy. Representative images are shown in the upper panels and the insets are magnified in the lower panels.

Figure 4. *Characterization of patient skin fibroblasts bearing the c.497_498del mutation in TMEM70.* **A.** Scheme representing the truncated version of TMEM70 resulting from the *c.497_498del* mutation leading to premature stop codon p.Tyr166Cysfs*7. MTS: Mitochondrial Targeting Sequence. TM: Transmembrane segment. **B.** Isolated mitochondria from cultured fibroblasts of the patient and a control individual were lysed and proteins were separated by SDS-PAGE and analyzed by western blot. **C.** Total protein extracts from control fibroblasts and patient fibroblasts expressing TMEM70 or TMEM70-FLAG where indicated were separated by SDS-PAGE and analyzed by western blot. Contaminant signal surrounded by * represents residual signal from Su.d in the subsequent decoration of TMEM70. **D.** Patient fibroblasts expressing TMEM70 (P+TMEM70) or GFP as a control (P) were fixed, sliced and imaged by TEM. Representative images are shown.

Figure 5. *TMEM70 targets specifically the subunit c of the ATP synthase.* **A.** Isolated mitochondria from 143B cell line containing (Rho$^+$) or not (Rho°) mitochondrial DNA were lysed and proteins were separated by SDS-PAGE and analyzed by western blot. **B.** Total protein extracts from 143B cell line containing (Rho$^+$) or not (Rho°) mitochondrial DNA expressing the indicated constructs were separated by SDS-PAGE and analyzed by western blot. **C.** HEK293T cells were transduced with shRNA constructs to knock-down TMEM70 (sh-TMEM70) and/or ATP5B (sh-β). Non-transduced HEK293T were used as control. Total protein extracts were prepared, separated by SDS-PAGE and analyzed by western blot.

Figure 6. *Physical interaction between TMEM70 and the subunit c of the ATP synthase.* **A.** Immunoprecipitation of TMEM70-FLAG. Mitochondria isolated from TMEM70-KO cells overexpressing TMEM70-FLAG, or TMEM70 as a control, were used in immunoprecipitation assays using anti-FLAG M2 magnetic beads. Digitonin extractions were performed in order to preserve protein-protein interactions. Extraction supernatants (S) represent the input material incubated with the beads while insoluble pellet (P) were set apart for analysis. The unbound material come with the flow-through (FT) while bound proteins are retained on the beads and further eluted (E) natively by competition with free 3xFLAG peptide. Portions (indicated at the bottom of the panel) of each fraction were analyzed by SDS-PAGE and western blot. The signals surrounded by * represent residual signal from Su.d in the subsequent decoration of TMEM70. **B-H.** Mitochondria were isolated for each cell line and subjected to digitonin extraction. The extracts were analyzed by BN-PAGE in a first dimension. The horizontal arrow above each panel indicated the migration direction. Some

lanes were used for in-gel ATPase activity assay where shown. All other lanes of the BN-PAGE were cut and analyzed by SDS-PAGE in a second dimension. Proteins were transferred to nitrocellulose and analyzed by western blot. Position of fully (CV) or partially (Vestigial CV) assembled ATP synthase, F1-c$_8$ subcomplex, F1-ATPase, and free Su.Beta, or TMEM70-containing complexes (*), are indicated below each panel with approximate calculated molecular weight in KDa above panels when applicable. **BC.** Analysis of original HEK293T and TMEM70 KO. The high molecular weight part of the 4-16% BN-PAGE lanes was cut in order to fit lanes till bottom in the SDS-PAGE 2D well. **D-G.** The low molecular weight part of the 3-12% BN-PAGE lanes was cut in order to fit lanes till top in the SDS-PAGE 2D well. **DE.** Analysis of TMEM70 KO expressing TMEM70-FLAG (D) or TMEM70 (E). These samples were loaded twice on the BN-PAGE. One lane was used for 2D western blot analysis and the second was used to reveal in-gel ATPase activity that is shown at the top of each panel. **FG.** Analysis of 143B cell line containing (Rho$^+$, F) or not (Rho°, G) mitochondrial DNA. **H.** Native eluates from the immunoprecipitation of TMEM70-FLAG described in A were analyzed by two-dimensional electrophoresis and western blot, as described above for mitochondrial extracts. TMEM70-Su.c complexes display different sizes (*), probably reflecting increasing incorporation of Su.c molecules.

Figure 7. *Submitochondrial localization of TMEM70 by fluorescence microscopy.* **A.** 143B-rho$^+$ cells expressing TMEM70 cDNA were fixed and immunostained with antibodies against Mitofilin/Mic60 (upper panel), or TMEM70 (lower panel). Confocal (left) and STED super-resolution (right) images are shown with insets magnified on the right panels. **B.** 143B-rho$^+$ cells expressing TMEM70-FLAG were fixed, immunostained with antibodies against Mitofilin/Mic60 (red) and FLAG (green), counter-stained with DAPI (blue), and subjected to expansion microscopy. A representative image is shown (left panel) with an inset magnified on the right panel in separate channels (upper right) and overlay (lower right). **C.** Cultured human skin fibroblasts were fixed, immunostained with antibodies against TMEM70 (green), and subjected to expansion microscopy. A representative image is shown on the left and the inset magnified on the top right corner. **D.** Scheme representing the relative localization of Mic60 (in red) and TMEM70 (in green) in the inner membrane sub-compartments. OM: outer membrane; IBM: inner boundary membrane; ICM: inner cristae membrane. Scale bars: 5 μm full size images, 500 nm zoomed images (D, 1μm).

Figure 8. *Model for the molecular action of TMEM70 towards the subunit c of the ATP synthase.* **A.** Molecular model for the TMEM70-dependent assembly of the c-ring. TMEM70 forms dimers that arrange in eight-copy structure in which each dimer can accommodate one Su.c in order to form the c-ring. After the c-ring is released, TMEM70 structural ring or disassembled dimers are involved in a new c-ring formation as indicated by the arrows. Approximate calculated molecular weights for each structure is indicated on the figure. **B.** The biogenesis of the ATP synthase is represented with a special focus on the c-ring. The Su.c precursor (in green) is imported into mitochondria through the protein translocases (grey cylinders) at the inner boundary membrane (IBM). The Su.c precursor gets processed by the Matrix Processing Peptidase (represented as scissors). TMEM70 (in red) forms dimers (TMEM70$_{dimer}$ or T$_d$) in cristae that interact with Su.c within higher order oligomers in order to form the c-ring. TMEM70 complexes release directly or disassemble into dimers to liberate the c-ring and take in charge new Su.c. The c-ring next assembles with premade F1

subcomplex and the additional subunits are added to form ATP synthase monomers, dimers, and oligomers.

Table 1. *Oligonucleotides used in this study.*

Primer name	Nucleotide sequence	Additional information
TMEM70-Fwd	5'GC<u>CTCGAG</u>**ATG**CTGTTTCTGGCGTTGGGGC	XhoI added cloning site underlined; TMEM70 start codon in bold
TMEM70-Rev-Stop	5'GC<u>GAATTC</u>**TCA**TTTGTCATCTTTATGCCGTTTCTC	EcoRI added cloning site underlined; TMEM70 stop codon in bold
TMEM70-Rev-NoStop	5'GC<u>GAATTC</u>**TTT**GTCATCTTTATGCCGTTTCTC	EcoRI added cloning site underlined
TMEM70-noSfi-Fwd	5'AGCGGGCCTTCGGG**A**CCGGTAGCCGGC	Mutated nucleotide in bold
TMEM70-noSfi-Rev	5'GCCGGCTACCGG**T**CCCGAAGGCCCGCT	Mutated nucleotide in bold
3xFLAG-Sense	5'<u>AATTC</u>GATTACAAGGATGACGACGATAAGGACTATAAGGACGATGATGACAAGGACTACAAAGATGATGACGATAAATGA<u>G</u>	Nucleotides for *Eco*RI and *Bam*HI cohesive ends, respectively, underlined
3xFLAG-Antisense	5'<u>GATCC</u>TCATTTATCGTCATCATCTTTGTAGTCCTTGTCATCATCGTCCTTATAGTCCTTATCGTCGTCATCCTTGTAATC<u>G</u>	Nucleotides for *Bam*HI and EcoRI cohesive ends, respectively, underlined
shT1-Fwd	5'<u>GATCC</u>**GGGAAGGATATGTTCGATTCTTAAA**TTCAAGAGA**TTTAAGAATCGAACATATCCTTCCC**TTTTT<u>G</u>	Target sequence in bold; nucleotides for *Bam*HI and *Eco*RI cohesive ends, respectively, underlined
shT1-Rev	5'<u>AATTC</u>AAAAA**GGGAAGGATATGTTCGATTCTTAAA**TCTCTTGAA**TTTAAGAATCGAACATATCCTTCCC**<u>G</u>	Target sequence in bold; nucleotides for *Eco*RI and *Bam*HI cohesive ends, respectively, underlined
shT2-Fwd	5'<u>GATCC</u>**CGAGTCTGATTGGCCTTACATTTCT**TTCAAGAGA**AGAAATGTAAGGCCAATCAGACTCG**TTTTT<u>G</u>	Target sequence in bold; nucleotides for *Bam*HI and *Eco*RI cohesive ends, respectively, underlined
shT2-Rev	5'<u>AATTC</u>AAAAA**CGAGTCTGATTGGCCTTACATTTCT**TCTCTTGAA**AGAAATGTAAGGCCAATCAGACTCG**<u>G</u>	Target sequence in bold; nucleotides for *Eco*RI and *Bam*HI cohesive ends, respectively, underlined
shT1-Fwd-pLV	5'<u>CGCGT</u>**GGGAAGGATATGTTCGATTCTTAAA**TTCAAGAGA**TTTAAGAATCGAACATATCCTTCCC**TTTTT<u>AT</u>	Target sequence in bold; nucleotides for *Mlu*I and *Cla*I cohesive ends, respectively, underlined
shT1-Rev-pLV	5'<u>CGAT</u>AAAAA**GGGAAGGATATGTTCGATTCTTAAA**TCTCTTGAA**TTTAAGAATCGAACATATCCTTCCC**<u>A</u>	Target sequence in bold; nucleotides for *Cla*I and *Mlu*I cohesive ends, respectively, underlined
shT2-Fwd-pLV	5'<u>CGCGT</u>**CGAGTCTGATTGGCCTTACATTTCT**TTCAAGAGA**AGAAATGTAAGGCCAATCAGACTCG**TTTTT<u>AT</u>	Target sequence in bold; nucleotides for *Mlu*I and *Cla*I cohesive ends, respectively, underlined
shT2-Rev-pLV	5'<u>CGAT</u>AAAAA**CGAGTCTGATTGGCCTTACATTTCT**TCTCTTGAA**AGAAATGTAAGGCCAATCAGACTCG**<u>A</u>	Target sequence in bold; nucleotides for *Cla*I and *Mlu*I cohesive ends, respectively, underlined
TMEM70_sgRNA-1 Fwd	5'<u>CACCG</u>**CACCCGCGTGATGCTGTTTC**	Target sequence in Exon 1 in bold; nucleotides for *Bsm*BI cohesive ends underlined
TMEM70_sgRNA-1 Rev	5'<u>AAAC</u>**GAAACAGCATCACGCGGGTG**<u>C</u>	Target sequence in Exon 1 in bold; nucleotides for *Bsm*BI cohesive ends underlined
TMEM70_sgRNA-2 Fwd	5'<u>CACCG</u>**CGCCCTACCTGCGCTCGACC**	Target sequence in Exon 1 in bold; nucleotides for *Bsm*BI cohesive ends underlined
TMEM70_sgRNA-2 Rev	5'<u>AAAC</u>**GGTCGAGCGCAGGTAGGGCG**<u>C</u>	Target sequence in Exon 1 in bold; nucleotides for *Bsm*BI cohesive ends underlined
TMEM70_sgRNA-3 Fwd	5'<u>CACCG</u>**ATTACTTACCAAACACTGCT**	Target sequence in Exon 2 in bold; nucleotides for *Bsm*BI cohesive ends underlined
TMEM70_sgRNA-3 Rev	5'<u>AAAC</u>**AGCAGTGTTTGGTAAGTAAT**<u>C</u>	Target sequence in Exon 2 in bold; nucleotides for *Bsm*BI cohesive ends underlined
TMEM70_sgRNA-4 Fwd	5'<u>CACCG</u>**GCTAATTTATACTGGCAATA**	Target sequence in Exon 2 in bold; nucleotides for *Bsm*BI cohesive ends underlined

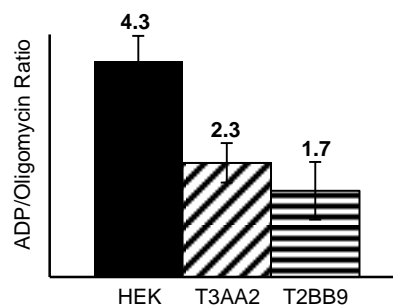|		
TMEM70_sgRNA-4 Rev	5'AAAC**TATTGCCAGTATAAATTAGC**C	Target sequence in Exon 2 in bold; nucleotides for *Bsm*BI cohesive ends underlined
TMEM70Ex1-Fwd	5'AAGCCGTGTCTCGCAGTCG	
TMEM70Ex1-Rev	5'TGGGAGAGGTCGCGAAGAGC	
TMEM70Ex2-Fwd	5'GTTGACCATAATGATCCCTG	
TMEM70Ex2-Rev	5'CTACATCTTATCAACACACCTC	

A

1   81   103   125 140   162   260

Cleavable MTS   P1   TM1   TM2   P2

B

Nuc   Mito   Micro   Cyto

Fibrillarin

Su.Beta

ERGIC p58

Actin

TMEM70

C

KCl 500 mM Na_2CO_3 pH 11,5

Pellet   Sup   Pellet   Sup

cyt *c*

VDAC1

TMEM70

D

+ PK   - PK

Swelling: +   -   +   -

Su.Beta

cyt *c*

TMEM70

E

IMS

IM

Matrix

N

C

Figure 1

A

B

C

D

E

Figure 2

A

TMEM70 KO clones

HEK293T | T2AC2 | T2AC11 | T2BB9 | T3AA2 | T3AG7 | T3BH6

TMEM70 *
Su.Alpha
Su.Beta
Su.b
Su.OSCP
CORE2
TOM20

B
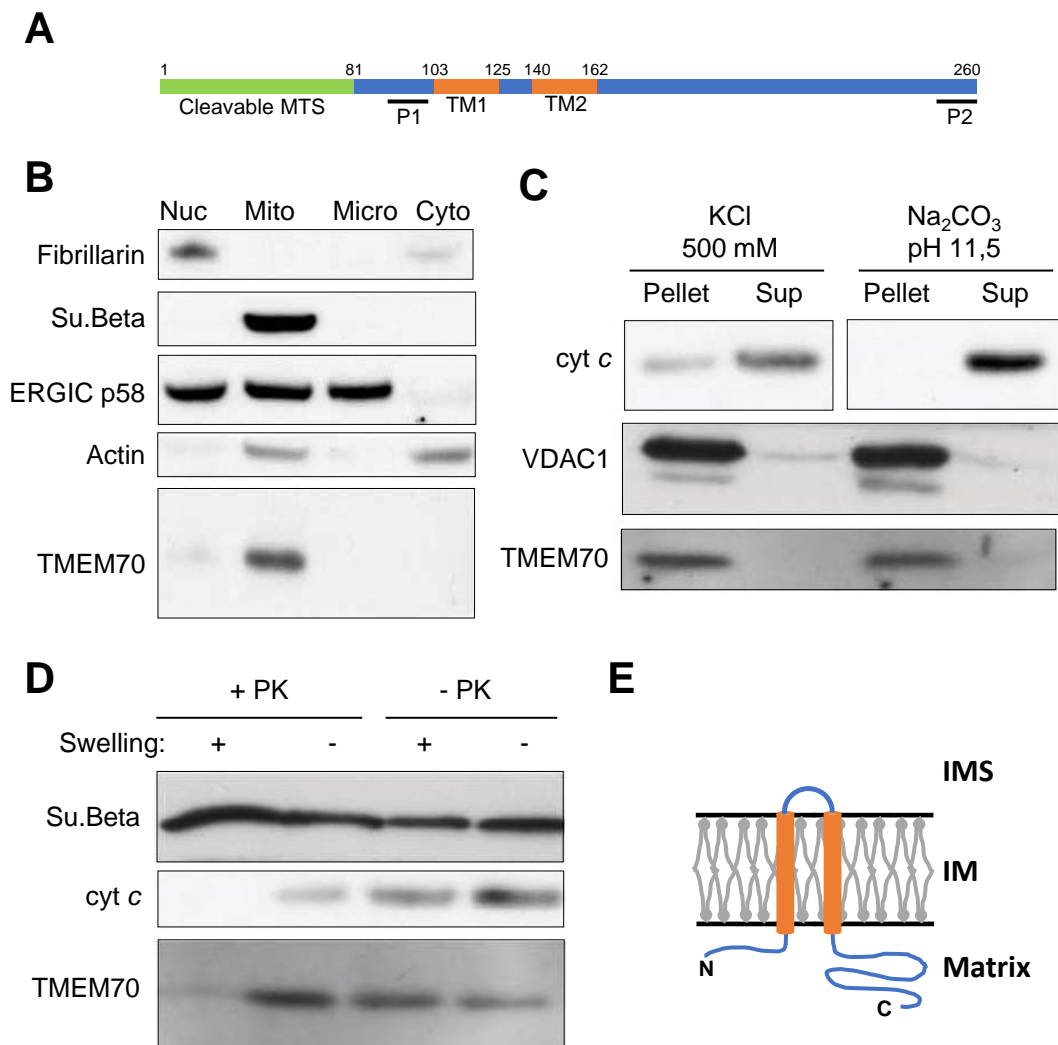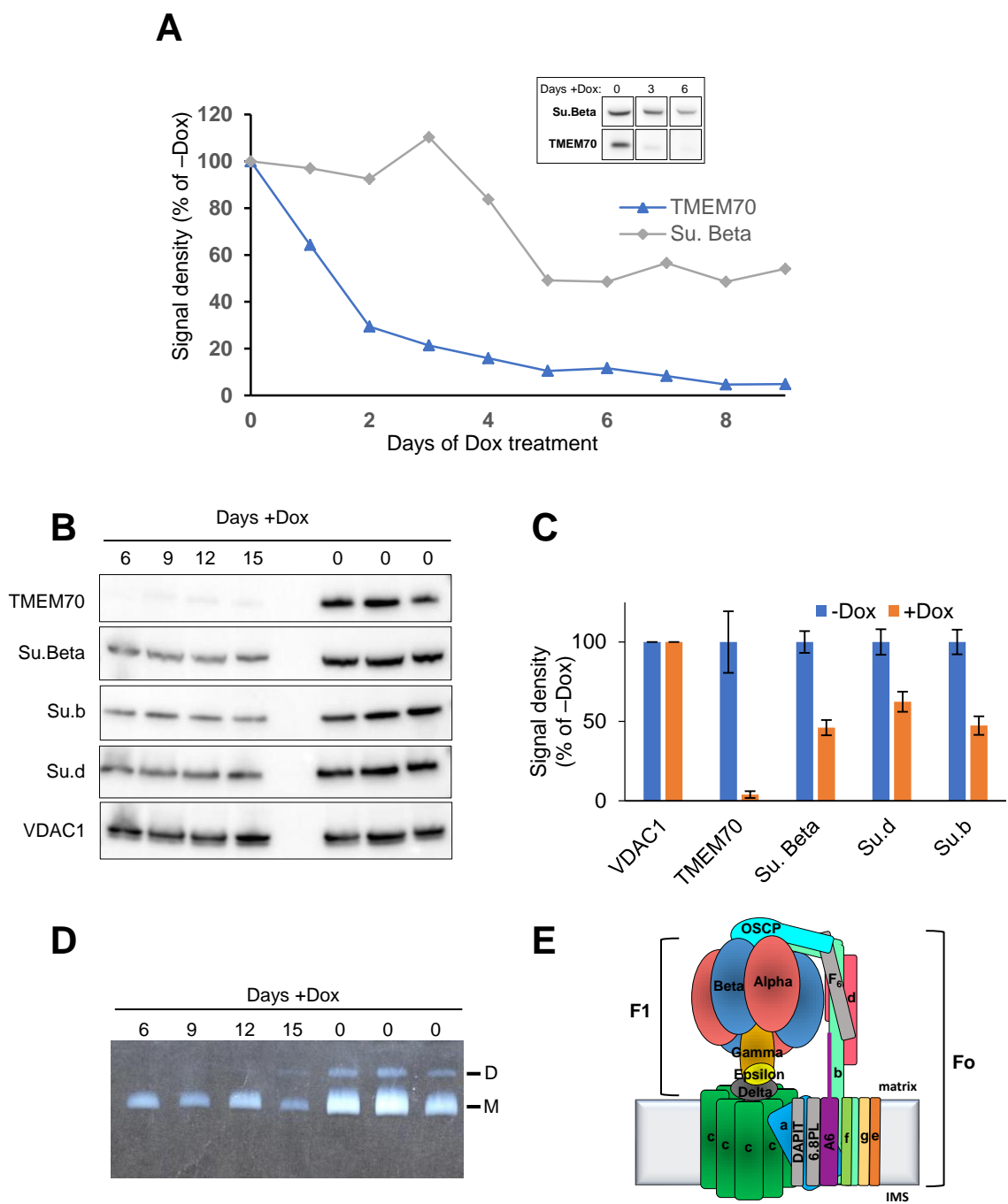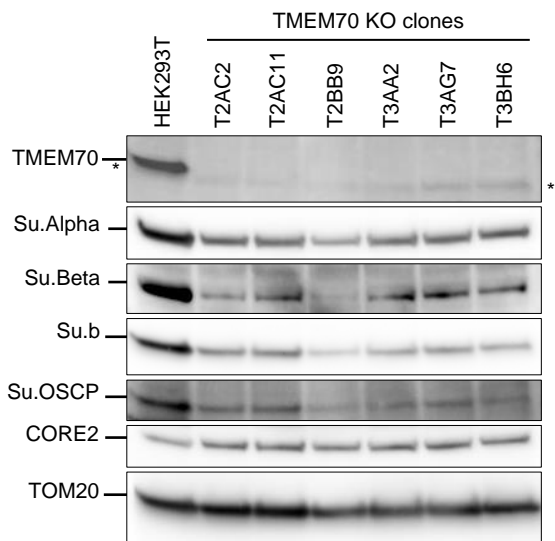
Respiratory Activity	HEK293T	T3AA2	T2BB9
ADP-stimulated	3.9+/-0.79	2.48+/-0.47	2.19+/-0.46
Oligomycin-inhibited	0.92+/-0.16	1.10+/-0.13	1.34+/-0.24
CCCP-uncoupled	8.38+/-1.93	7.33+/-1.07	7.35+/-0.85

C

ADP/Oligomycin Ratio

4.3 — HEK
2.3 — T3AA2
1.7 — T2BB9

D

HEK293T | KO+TMEM70 | KO

D
M

E

Not transduced | +TMEM70 | +TMEM70-FLAG | +Empty Vector

TMEM70-FLAG
TMEM70
Su.Alpha
Su.Beta
Su.b
Su.d
Su.OSCP
Su.c
NDUFB6
TOM20

ATP synthase related proteins

F

KO | KO + TMEM70

Figure 3

A

B

C

D

Figure 4

A

Rho⁺ Rho°

Su.c —

TMEM70 —

Su.d —

SDHA —

TOM20 —

B

Rho⁺ Rho°

+TMEM70-FLAG +TMEM70 +TMEM70-FLAG +TMEM70

Su.Beta —

Su.d —

Su.c —

TMEM70-FLAG —

TMEM70 —

C

HEK293T sh-β + sh-TMEM70 sh-β

Su.Beta —

Su.b —

Su.d —

Su.c —

TMEM70 —

NDUFB6 —

Figure 5

A

B

C

Figure 6

D

Su.Beta

TMEM70
-FLAG

Su.c

CV

*

E

Su.Beta

TMEM70

Su.c

CV

*

F

1200   600   450   380

Su.Alpha

Su.d

Su.b

TMEM70

Su.c

CV   F1

F1-c$_8$

*

G

550   450   380

Su.Alpha

TMEM70

Su.c

Vestigial CV   F1

F1-c$_8$

*

H

TMEM70-
FLAG

Su.c

*

Figure 6

Figure 7

A

B

Figure 8